Title

Next-generation anodes for high-energy and low-cost sodium-ion batteries

Journal

Nature Reviews Materials, 11(2)

ISSN

2058-8437

Authors

Zuo, Wenhua

Liu, Zaichun

Dopilka, Andrew

et al.

Publication Date

2026-02-01

DOI

10.1038/s41578-025-00857-4

Next-generation Anodes for High-Energy and Low-Cost Sodium-Ion Batteries

Wenhua Zuo[1,12,13], Zaichun Liu[2,3,12,13], Andrew Dopilka[4,12], Ziqi Yang[5,12], Yuqi Li[2,3,12], Joseph Kubal[1,12], Haegyeom Kim[6,12], Fang Liu[5,7,12], Ping Liu[8,12], Anh T. Ngo[9,12], Johanna Nelson Weker[10,12], Zonghai Chen[1,12], Robert Kostecki[4,12], Julie Wulf-Knoerzer[12], Venkat Srinivasan[1,12], Yi Cui[2,3,11,12]*, Khalil Amine[1,12]*, Gui-Liang Xu[1,12]*

[1] Chemical Sciences and Engineering Division, Argonne National Laboratory, Lemont, IL, USA

[2] Stanford Institute for Materials and Energy Sciences, SLAC National Accelerator Laboratory, Menlo Park, CA, USA

[3] Department of Materials Science and Engineering, Stanford University, Stanford, CA, USA

[4] Energy Storage and Distributed Resources Division, Lawrence Berkeley National Laboratory, Berkeley, CA, USA

[5] Department of Chemical and Biological Engineering, University of Wisconsin−Madison, Madison, WI, USA

[6] Materials Sciences Division, Lawrence Berkeley National Laboratory, Berkeley, CA, USA

[7] Department of Materials Science and Engineering, University of Wisconsin−Madison, Madison, WI, USA

[8] Department of Nanoengineering, University of California, San Diego, La Jolla, CA, USA

[9] Department of Chemical Engineering, University of Illinois at Chicago, Chicago, IL, USA

[10] Stanford Synchrotron Radiation Light source, SLAC National Accelerator Laboratory, Menlo Park, CA, USA

[11] Department of Energy Science and Engineering, Stanford University, Stanford, CA, USA

[12] Low-cost and earth-abundant Na-ion Storage (LENS) consortium, Lemont, IL, USA

[13] These authors contributed equally to this work

* Correspondence to: yicui@stanford.edu (Y.C.); amine@anl.gov (K. A.); xug@anl.gov (G.-L. X)

Abstract

Sodium-ion batteries (NIBs) are increasingly becoming commercially viable alternatives to lithium-ion batteries (LIBs), driven by sodium's lower cost and greater resource availability. However, current NIB technology still falls short of established LIB systems, such as those based on $LiFePO_4$, in both cost efficiency and energy density. Since the early 2020s, industrial advances have raised NIB energy densities to around 175 Wh kg^{-1}, performance still remains limited by the relatively low specific capacity (typically 200–350 mAh g^{-1}) and low tap density (0.3-1.0 g cm^{-3}) of the prevailing hard carbon anodes. This Review analyzes emerging anode materials that could unlock higher energy and lower cost NIBs, with a focus on high-capacity hard carbon and alloy-based systems. We discuss the latest progress, fundamental challenges, and future directions in these anode materials across the key themes of electrode design, structure–property engineering, and characterization. By offering forward-looking insights into the rational design and optimization of anode materials, this Review aims to accelerate the R&D of commercially viable NIBs and support the broader advancement of energy storage technologies.

ToC blurb

Sodium-ion batteries are promising low-cost alternatives to lithium-ion systems yet limited by underperforming anodes. This Review highlights advances and challenges in hard carbon and alloy-based anodes, outlining design strategies to boost capacity, stability, and commercial viability of next-generation high-energy sodium-ion batteries.

[H1] Introduction

Sodium-ion batteries (NIBs) are emerging as viable alternatives to lithium-ion batteries (LIBs), driven by sodium's natural abundance and widespread availability.[1–3] However, compared to lithium-based systems, the larger ionic radius of Na^+, lower capacity and pronounced phase transitions of sodium-based cathodes, and lack of high-performance anode materials have hindered the development and commercialization of NIBs.[4–6] Since the early 2020s, progress in commercializing room-temperature NIBs by battery manufacturers such as CATL, TIAMAT and HiNa Battery[7–11], as well as the deployment of grid-scale storage stations[12,13], have transitioned NIBs from early-stage research toward real-world implementation (Figure 1a). Large consortium-led R&D efforts have also been established to accelerate electrode discovery and cell development. These milestones have prompted researchers, industry leaders, and policymakers to critically re-evaluate the potential of NIBs to evolve from a secondary alternative into a dominant technology for large-scale energy storage.[14–17]

NIBs share the same cell design as LIBs, with a cathode, an anode, and an electrolyte.[18] Many LIB electrode materials have sodium-based analogues. For instance, the layered O3-$LiNi_xCo_yMn_{1-x-y}O_2$ cathode in LIBs has a structural counterpart in O3-$NaNi_xCo_yMn_{1-x-y}O_2$ (or the more prevailing O3-$NaNi_xFe_yMn_{1-x-y}O_2$),[19–22] whereas polyanion $LiFePO_4$ (LFP) in LIBs corresponds to $Na_3V_2(PO_4)_3$ in NIBs.[23–25] Although sodium-based cathodes generally exhibit lower energy density than lithium-based alternatives, they present a clear cost advantage, benefitting from the availability of low-cost Fe- and Mn-based materials with strong electrochemical reversibility.[26] Advances in electrolyte development have further unlocked the electrochemical potential of NIB cathodes, allowing them to approach their intrinsic energy storage properties.

Nonetheless, considerable challenges persist on the anode side. Currently commercialized, electrochemically stable hard carbon (HC) anodes deliver limited specific capacities (typically 200–350 mAh g^{-1}), with much of the capacity lying within the sloping region of the voltage

profile.[27–29] This limitation leads to two critical issues.[30] First, this voltage profile confines a large portion of capacity to the low-voltage range, which lowers the full-cell energy density and hinders efficient utilization at high charge rates. Second, the relatively low energy density of HC at the material level necessitates larger quantities of both cathode and anode materials in full-cell configurations,[30] driving up manufacturing costs. In parallel, alternative anodes such as sodium titanates (for example, $Na_2Ti_3O_7$) offer excellent structural stability and safe operating potentials (~0.3–0.8 V vs Na^+/Na),[31–33] making them suitable for stationary storage or applications requiring long service life and reliability. However, their relatively low capacity (100-230 mAh g^{-1}) strongly limits their commercial viability in high-energy NIBs, where maximizing specific energy remains a key priority.

In this Review, we systematically examine the two main critical directions for developing the next generation of anode materials for high-energy NIBs. The first targets high-capacity HC, aiming for a reversible capacity of ≥ 400 mAh g^{-1} while achieving a stable low-potential plateau with improved Na ion diffusivity. The second centers on alloy-based anodes, exemplified by P, Sn and Pb, which deliver considerably higher theoretical capacities than HC. We provide a comprehensive assessment of recent progress, potential applications, and key challenges in advancing high-energy and low-cost NIBs.

[H1] Strategic roadmap for anode design

Rational design of the anode material is a decisive factor in achieving high-energy and economically competitive NIBs. Figure 1b quantitatively illustrates the projected cell-level energy metrics of NIBs equipped with varying proportions of HC and alloy-based anodes, derived from BatPaC (Battery Performance and Cost Modeling) simulations.[34] The commercial LFP/graphite LIB system has been used as a techno-economic benchmark (orange shaded region), which is projected to reach < \$51 kWh^{-1} by 2030.[35]

HC remains the mainstream anode material for commercial NIBs, offering practical capacities of 200-350 mAh g^{-1}. As shown in Figure 1b, when paired with layered oxide cathode—$NaNi_{0.33}Fe_{0.33}Mn_{0.33}O_2$ with a baseline specific capacity of 125 mAh g^{-1}—the cell-

level energy densities reach ~140–160 Wh kg^{-1} and ~260–280 Wh L^{-1}, falling short of current industrial LFP/graphite LIBs (170-180 Wh kg^{-1} and 330-350 Wh L^{-1}). To achieve parity with LFP systems in terms of energy density, the anode capacity must be substantially increased. Developing high-capacity HC anodes reaching 450 mAh g^{-1} or incorporating high-capacity alloy materials such as tin (847 mAh g^{-1}) or phosphorus (P, 2596 mAh g^{-1}) into the HC matrix are viable strategies. As shown in the plot, a 50% Sn–HC composite elevates the cell energy density to ~170 Wh kg^{-1} and ~340 Wh L^{-1}, and further increasing the Sn content to 75% or higher pushes the metrics beyond 175 Wh kg^{-1} and ~360 Wh L^{-1}. Similar improvements are observed for P-based composites, where a 50% P anode also enables LFP-equivalent energy densities.

It is worth noting that in practical applications, enhancing the cathode capacity and durability is equally essential to boost full-cell energy density. Although many current commercial layered oxides (mainly $NaNi_xFe_yMn_{1-x-y}O_2$) operate at ~120-135 mAh g^{-1}, advancing to next-generation cathodes with capacities of 150, 180, or even 200 mAh g^{-1} will be necessary to unlock higher energy metrics. Cu-containing layered oxides are particularly attractive, as they simultaneously offer increased energy density and improved air stability.[5,6,36,37] Additionally, dual-phase cathodes such as P2–O3 intergrowths,[38,39] optimized cation distribution,[20,40] and solvent-mediated lattice engineering[41] have been effective in improving Na^+ transport and cathode reversibility, further supporting progress toward high-performance sodium-ion full cells. Indeed, the Naxtra battery announced by CATL in April 2025, which delivers a cell-level energy density of up to 175 Wh kg^{-1}, highlights the importance of both high-capacity cathodes and anodes in bridging the gap with LFP-based lithium-ion systems.

These trends suggest that, to match or surpass LFP/graphite energy densities without structural or packaging innovations, NIBs generally require an average anode capacity of ~400–450 mAh g^{-1}. This target can be approached via multiple routes including high-capacity alloys, optimized hard carbons with pre-sodiation, or hybrid/composite designs. Among them,

strategic alloy integration, for example incorporating substantial fractions (≥50%) of Sn or P—offers a practical path to reach the required capacities.

[H1] Hard carbon anodes

Carbon-based materials are leading candidates for industrial electrochemical intercalation batteries, as evidenced by the successful implementation of graphite in LIBs.[42,43] However, de-solvated Na^+ ions do not readily intercalate into graphite owing to the thermodynamic instability of sodium intercalation compounds (sodium-graphite binary compounds).[44]

Instead, non-graphitizable HC has emerged as the leading anode candidate for NIBs. The concept of sodium storage in HC was first demonstrated in 2000 using glucose-derived carbon, which exhibited a reversible capacity exceeding 300 mAh g^{-1} and a low operating plateau potential near 0 V vs. Na^+/Na.[45] The dual-region voltage profile—comprising a sloping region followed by a flat plateau—is now widely considered a distinctive feature of HC-based anodes. HCs are characterized by disordered amorphous structures with turbostratic layers, enlarged interlayer spacing, and nanoscale porosity comprising both open and closed pores (Figure 2a).[28]

The complexity of HC microstructures has fueled ongoing debate over the mechanisms of sodium storage. Three dominant storage contributions are generally recognized: capacitive adsorption, nanopore filling, and interlayer insertion (Figure 2b).[45–53] Capacitive adsorption, primarily associated with the sloping region, is influenced by intrinsic defects[48] and heteroatoms[49,50] in the carbon material. The low-potential plateau region is often attributed to Na^+ insertion within carbon interlayers or pore-filling processes, both of which are believed to be closely linked to the HC's interlayer *d*-spacing and pore size.[45–47,49–53] Yet, the interplay among these Na storage mechanisms remains contentious, as reflected in competing conceptual models such as "insertion–absorption",[45] "adsorption–insertion",[51] "adsorption–nanopore filling"[52] and "absorption–nanopore filling and insertion"[53]. The exact relationship between these storage mechanisms and the synthetic processes that shape HC microstructure is still unclear. Additionally, the precise chemical state of stored sodium—whether ionic[54] or metallic[55–57]—remains debated, underscoring the need for advanced operando and spatially resolved characterization techniques to better understand sodium storage behaviors in HC

microstructures.

Research on HC anodes spans both academic and industrial efforts, with key priorities including the selection of precursors, synthesis optimization, control of microstructure, and elucidation of the fundamental mechanisms of sodium storage. Achieving electrochemical breakthroughs, such as a capacity target of ≥ 450 mAh g^{-1}, alongside high initial Coulombic efficiency (ICE) and outstanding cycle life, remains essential for commercial viability.

[H2] Precursors and processing

The microstructure of HC is strongly influenced by the nature of its precursors (Figure 2c), which determine key parameters such as interlayer distance, pore structure, and defect distribution. Precursors derived from biomass (such as wood[58–60] and plant residues[61–67]), synthetic polymers (such as polyvinyl alcohol[68] and resins[69–71]), natural organic compounds (such as sugars[72–74] and starches[75]), and fossil-based sources (such as coal and pitch)[76] have been widely investigated. The broad availability of these precursors has driven extensive research into HC anodes, [catalyzing advances in their material design that have boosted?]specific capacities [in a few cases?] to 300-500 mAh g^{-1} [58–67,76,77]. [The fact that such high capacities are achievable?] has strengthened the prospects of HC as a practical anode material for high-energy NIBs.

Thermal treatment protocols—specifically pre-oxidation and pyrolysis—also define the resulting HC structure (Figure 2c).[78,79] The dehydrogenation, condensation, aromatization, and carbon framework rearrangements that occur during pyrolysis dictate features such as graphitization degree, interlayer spacing, pore size and morphology, and surface functionalities and properties.[28,80] Treatment parameters including carbonization temperature,[78,81] heating rate,[79] and duration[82] critically modulate these outcomes. Moreover, purification and pre-treatments (for example, hydrothermal processing,[72] microwave irradiation,[48,83,84] and water, acid, or base washing[85,86]) offer additional levers for tuning nanostructure and sodium storage behavior.

Innovative processing techniques—such as Joule heating,[87] spark plasma sintering,[88,89] and microwave induction heating[90]—offer potential for rapid synthesis and structural control.

However, challenges remain in regulating reaction temperatures, establishing reliable structure–processing correlations, and scaling up for industrial applications. Streamlined production processes and scalable manufacturing technologies will be essential for realizing the practical applications of HCs.

[H2] Advanced strategies for increasing capacity

Beyond precursor selection and pyrolysis optimization, considerable research has focused on increasing the sodium storage capacity of HCs by tailoring their structural features in both the sloping and plateau regions of the voltage profile.[48–50,70,91–94] The sloping region, dominated by capacitive adsorption, has been improved by strategies such as heteroatom doping,[7,8] defect engineering,[48] and low-temperature carbonization[92]. These modifications introduce additional adsorption sites by increasing structural disorder or introducing polar functional groups. At the same time, however, they often lead to a reduction in ICE due to irreversible sodium trapping and increased reaction barriers. Indeed, balancing slope-type capacity and ICE remains a critical challenge for hard carbon anodes. Strategies that fine-tune the above modifications, including lowering the carbonization temperature[95] and optimizing heteroatom configurations,[96] have notably improved this balance. Additionally, defect engineering and solid electrolyte interphase (SEI) tailoring have been shown to enhance Na^+ diffusion kinetics and interfacial stability, enabling a more favorable trade-off between slope capacity and ICE.[97] These advances highlight the importance of mechanistic understanding and targeted structural tuning to improve the practical viability of slope-dominated carbon materials.

In contrast to slope-region optimization, improving plateau capacity is considered more important for achieving high energy density,[67,87] as it is closely associated with insertion and Na cluster formation reactions within the carbon structure (Figure 2d). One effective strategy involves expanding the interlayer spacing to better accommodate Na^+ ions. Heteroatom doping with elements such as phosphorus,[70,91,93,94] sulfur,[94,98] potassium,[99] calcium[100] and others has been shown to enlarge the *d*-spacing, facilitating Na^+ insertion and improving plateau capacity.

Micropore manipulation, particularly the formation of closed nanopores, has emerged as another key design principle to promote nanopore-filling–dominated sodium storage (Figure

2d). [63,101] Methods developed to control microporosity include low-temperature hydrogen reduction,[102] pre-oxidation (such as hot air exposure[103–105] or plasma treatment[106]), and template-assisted porosity control. Various templating and etching agents—including ethanol,[107] liquid salt,[108] MgO particles,[109] KOH,[110] Zn single atoms,[111] graphene oxide,[112] carbon dots,[113] organic polymers such as poly(vinyl butyral),[114] CO_2,[75] and ZnO[115]—have been utilized to generate hierarchical pore structures. Chemical activation and catalytic carbonization can further tune pore characteristics.[110] The introduction of metal ions such as Ni^{2+},[116] Fe^{3+},[117] Mg^{2+},[118] and Mn^{2+}[119] during carbonization can modulate the thermal decomposition pathways and favor micropore formation. In addition, coating technologies, such as chemical vapor deposition (CVD),[120,121] have been employed to convert open pores into closed ones, increasing sodium storage sites while suppressing unwanted side reactions.

Several of these strategies have been shown to regulate both interlayer spacing and microporosity and have synergistically elevated the reversible capacity of HCs to 400–600 mAh g^{-1} (Figure 2e).[83,84] This advancement raises the projected energy density of full NIBs to 200–300 Wh kg^{-1}, potentially rivaling or surpassing that of LFP-based LIBs.

Ultimately, achieving high capacity, good rate capability, and high ICE in HC anodes requires a holistic combination of material design strategies. Pore structure engineering tailors the size and distribution of micro- and mesopores to balance capacity and rate performance while minimizing irreversible Na^+ trapping. Heteroatom doping improves electronic conductivity, introduces additional active sites, and increases interlayer spacing to facilitate ion transport. Surface modification, including protective coatings and functional group introduction, enhances electrode–electrolyte compatibility, suppresses side reactions, and contributes to the formation of a stable SEI, thereby improving ICE and cycling stability. In parallel, electrolyte optimization and interfacial engineering, especially the formation of robust SEI, are critical for stabilizing electrode/electrolyte interfaces and improving long-term cycling performance.[122–125]

[H2] Challenges and outlook on HC anodes

Despite encouraging progress in the last […] years, several critical challenges continue to

impede the rapid development and large-scale commercialization of HC anodes for NIBs. Overcoming these multifaceted challenges requires coordinated efforts across materials design, process engineering, and device integration.

A major concern is the selection and standardization of precursors. Biomass-derived HCs are abundant and readily accessible, but their variability in composition and structure complicates precursor screening and supply-chain stabilization. Pitch-derived precursors offer much better batch-to-batch consistency and industrial scalability. Micropore engineering further boosts their performance, enabling capacities over 400 mAh g^{-1}.[126–128] [Yet their reliance on fossil fuels means they are not sustainable?] To ensure product uniformity and reproducibility, rigorous screening protocols and standardized precursor systems will need to be established. Beyond sourcing sustainable raw materials for supply chain security, key factors such as scalability, cost-effectiveness, and material stability must also be addressed by optimizing syntheses to improve yield and reduce energy consumption, adopting scalable fabrication techniques, and ensuring batch-to-batch consistency in structure and performance.

Another unresolved issue is the intrinsic complexity of HC microstructures, which obscures the sodium storage mechanism and hinders rational design. Disentangling the relative contributions of interlayer insertion, nanopore filling, and surface adsorption—especially under real-time sodiation conditions—requires advanced multiscale, operando characterization techniques, including cryogenic electron microscopy (cryo-EM), nuclear magnetic resonance (NMR) spectroscopy, and small-angle X-ray scattering (SAXS). Moreover, translating improvements in capacity and ICE to high-rate capability and long-term cycling stability is far from trivial.[47] Structural enhancements that increase capacity may impede ion mobility or compromise electrode integrity. Strategies to maintain robust ion diffusion networks, mechanically stable architectures, and interface resilience are needed to ensure durability under extended cycling and fast-charging conditions.

Achieving high energy density under practical conditions remains a major hurdle. Most reported high capacities are measured at low areal loadings (~1.0 mg cm^{-2}), which fall short of commercial relevance. However, as electrode thickness increases with higher active material

loadings, performance degrades owing to several interconnected issues: First, mechanical fragility increases, making thick HC electrodes more prone to cracking and pulverization at both pristine states and repeated charge-discharge. Second, ionic transport becomes limited due to poor electrolyte infiltration through the dense bulk, leading to increased overpotentials and sluggish kinetics. Moreover, electronic conductivity across the electrode thickness often becomes insufficient, resulting in non-uniform current distribution and partial utilization of active material.[129–131] To address these challenges, researchers are engineering HC electrodes with hierarchical porosity, often introduced via templating or controlled pyrolysis, to enhance ion accessibility while maintaining volumetric energy density.[132] The efforts to improve specific capacity often compromise ICE due to an increase in defects and irreversible (de-)sodiation.[83] A balanced approach integrating microstructural optimization, defect engineering, and controlled SEI formation is needed to simultaneously enhance capacity and efficiency. Simultaneously, incorporating high-performance binders and conductive additives helps establish continuous ion/electron transport pathways and reinforces mechanical integrity.[133] Additionally, surface modification of current collectors and textured electrode fabrication have been explored to reduce interfacial resistance and support uniform charge distribution.[134–140]

[H1] Alloy-based anodes

Silicon (Si) is widely recognized as a benchmark anode for next-gen LIBs, owing to its ultrahigh theoretical capacity of 4200 mAh g^{-1}.[141] However, the kinetically unfavorable Na–Si alloying process renders nanocrystalline or micro-sized Si largely electrochemically inactive in NIBs.[142,143] Although theoretical studies predict a capacity of 725 mAh g^{-1} for amorphous silicon (a-Si),[144] experimental results have been consistently far from satisfactory.[145–147] For instance, a-Si with particle sizes smaller than 100 nm exhibited reversible capacities around 340 mAh g^{-1}, along with a sloping voltage profile and rapid capacity fading upon cycling.[145] Silicate oxides show specific capacities of only about 200 mAh g^{-1}.[148] These limitations arise primarily from sluggish sodium kinetics, low Coulombic efficiency, and poor structural reversibility.[146,149]

In contrast to silicon, several alloy-based anodes, including phosphorus (P),[150–153] germanium (Ge),[154–156] tin (Sn),[142,157–160] antimony (Sb),[161–163] lead (Pb)[164–166], and bismuth (Bi)[167–169] have gained considerable attention for their more favorable Na-alloying thermodynamics and high theoretical capacities. Importantly, insights gained from the design and engineering of alloy-based anodes also inform the development of sodium metal and even anode-free battery chemistries.[170,171]

[H2] Structures, techno-economics and electrochemistry

Figure 3a–h[172,173] and Table 1 illustrate the structural diversity of various anodes for NIBs, emphasizing differences in atomic configurations and crystallographic symmetry. Among these materials, HC (Figure 3a) and P-based anodes (Figure 3b,c) stand out for their disordered frameworks and high structural adaptability. Red P exists in two forms: the industrially dominant amorphous phase (Figure 3b), which comprises randomly entangled P–P chains whose lack of long-range order provides abundant free volume and multidirectional diffusion pathways, effectively buffering mechanical stress during sodiation. In contrast, crystalline red phosphorus (space group C222) features a more compact one-dimensional chain network, which restricts Na^+ accessibility due to limited interstitial space and sluggish ion transport, resulting in inferior electrochemical activity. Accordingly, amorphous red P is the relevant form used in anodes. Black phosphorus (Figure 3c, space group: Cmca) adopts a two-dimensional layered configuration, where strong in-plane covalent bonding and weak interlayer van der Waals (vdW) interactions allow for rapid Na^+ transport along the layers and moderate accommodation of volume expansion. Despite their structural advantages, both red and black phosphorus suffer from low intrinsic electronic conductivity and substantial volumetric changes upon alloying, necessitating further structural engineering for practical implementation.

In contrast to these non-metallic systems, alloy-type anodes of Ge (Figure 3d), Sn (Figure 3e), and Pb (Figure 3f) possess dense, three-dimensional crystalline frameworks wherein atoms are typically tetrahedrally or octahedrally coordinated and form isotropic bonding networks. During sodiation, these structures undergo multi-step phase transitions, which are accompanied

by extreme volumetric expansion of up to 400%. In contrast, Sb (Figure 3g) and Bi (Figure 3h) (both in R-3m space group) adopt A7-type rhombohedral structures characterized by pseudo-layered arrangements. Each atom is geometrically sixfold coordinated, but only three atoms form strong and directional covalent bonds, while the other three atoms are weakly interacting, giving rise to anisotropic bonding. This anisotropic bonding not only promotes directional Na^+ diffusion but also offers interlayer spacing that can partially accommodate moderate volume changes during alloying to form Na_xSb or Na_xBi phases.

P-carbon composites have demonstrated practical capacities exceeding 2000 mAh g^{-1} (Table 1).[150,174,175] For example, a black P/ketjenblack–multiwalled carbon nanotube composite delivered over 2000 mAh g^{-1} with excellent cycling stability.[150] Sn-based anodes have also shown reversible capacities ranging from 860 to 878 mAh g^{-1}, making them highly promising for practical applications. Other candidates, such as Ge, Pb, Sb, and Bi, also exhibit capacities strongly surpassing that of HC (see Table 1). Hybridizing these active elements has emerged as a strategy to synergistically enhance capacity and cycling performance.[163,176,177]

Despite these benefits, severe volume expansion during sodiation remains a key obstacle (Figure 4a). For instance, P and Sn undergo volumetric expansion exceeding 400%,[155,157,158,178] and Pb and Sb expand by ~380%.[165] These drastic changes result in mechanical degradation, particle pulverization, and dynamic surface reconstruction, which collectively destabilize the SEI and accelerate capacity fading over cycling. Fortunately, in practical electrode architectures, such as Sn–C composites, the observed electrode-level expansion is substantially mitigated by the high density of Sn and the buffering effect of the carbon matrix.[179]Considering the trade-offs between theoretical capacity, elemental abundance, and environmental impact, red P and Sn are currently the most suitable alloy-type anode materials for practical NIB applications. Red P possesses an exceptionally high theoretical capacity of 2596 mAh g^{-1}, is earth-abundant (~1000 ppm in the Earth's crust), and benefits from large-scale industrial production with relatively low toxicity. Sn offers a high capacity of 847 mAh g^{-1}, along with favorable electrical conductivity, mechanical robustness, and excellent compatibility with conventional electrode processing. In contrast, Sb, Bi, Pb, and Ge suffer from low natural

abundance, environmental toxicity, or limited scalability, which pose substantial barriers to practical implementation. The practical deployment of Sb and Bi is limited by geochemical scarcity: Sb (0.2 ppm) and Bi (0.0085 ppm) are among the rarest elements in the Earth's crust (Figure 3i).[180] *Ge is similarly constrained by limited production (Figure 3j), and Pb faces significant environmental concerns. In stark contrast, P exhibits a unique combination of structural versatility, high natural abundance (~1000 ppm, 500 folds higher than Sn), and enormous global production scale (>2 × 10^8 t $year^{-1}$).[H2] Nano-structuringStrategies to stabilize structure*

[H3] Nano-structuring

One promising approach to mitigate these severe changes in volume involves engineering these materials at nanoscale (Figure 4b).[181] Nanostructured particles offer several advantages over the bulk: shortened Na^+ diffusion paths, larger surface area for electrochemical reactions, and enhanced mechanical tolerance toward volume fluctuations.[182,183] These benefits contribute to improved rate performance and cycling life.[161,184–187] For example, red phosphorus embedded in carbon nanofibers has demonstrated a reversible capacity of ~1850 mAh g^{-1} and stable cycling over 500 cycles, attributed to the suppression of P–electrolyte side reactions by the carbon framework.[175] Further enhancement can be achieved by constructing hybrid nanostructures combining active alloy elements with carbon matrices, conductive polymers, or secondary phases (Figure 4c). These designs buffer volume change, enhance electrical conductivity, and stabilize interfaces during cycling.

Scaling up nanostructured materials remains a major hurdle. Challenges include low tap density, high energy input during synthesis, use of expensive or hazardous reagents, and the requirement for sophisticated processing equipment. These factors complicate the transition from proof-of-concept research to cost-effective, industrial-scale manufacturing.

[H3] Micro-structuring

Compared to nanostructured materials, micron-sized alloy anodes offer several advantages.[188] Their lower surface area minimizes parasitic side reactions, contributing to more stable SEI

formation. In addition, higher tap density and better processability of micromaterials enable denser electrode packing and reduced manufacturing costs, both of which are critical for scaling up.[188,189] These attributes make micro-scale alloy materials attractive for practical applications, where volumetric energy density is a key metric.

However, micro-sized alloys face considerable challenges. In addition to severe mechanical stress and particle fracture, the longer ion and electron transport paths in bulk particles often limit rate capability and cycling performance. To address these issues, hierarchical or multiscale architectures have been explored.[190] By embedding micro and nanoscale active domains into a structural framework, such designs enable fast reaction kinetics and accommodate volume changes, while the larger skeleton provides mechanical stability and suppresses particle agglomeration (Figure 4d).[132,191,192]

Surface engineering and heteroatom doping offer further improvements. Carbon or oxide coatings stabilize the electrode–electrolyte interface, while doping with transition metals (such as Fe, Ti, Cu), non-metals (such as B), or oxides (such as TiO_2) can tune the alloy's electrochemical behavior (for example, potential) and enhance its mechanical properties.[163,187,193–198] These morphological and compositional modifications help mitigate irreversible capacity loss and improve both structural integrity and long-term cycling performance. Ultimately, bridging the gap between nanostructured resilience and micro-scale manufacturability could unlock the full potential of alloy anodes in practical NIBs.

[H3] Electrolyte modulation

The design of suitable electrolytes is important to stabilizing high-capacity alloy anodes. Electrolyte selection, including solvents, salts, additives, and their concentrations greatly influences ion transport, SEI chemistry, and cycling stability.[199–201]

Different solvents, such as ether-, sulfone-, and carbonate-based systems, can exhibit substantial differences in ion transport, SEI formation, viscosity, and thermal stability. Carbonate-based electrolytes (for example, ethylene carbonate (EC), propylene carbonate (PC), and diethyl carbonate (DEC)) have been widely used in LIBs and have also shown

compatibility with alloy anodes in NIBs. In a study quantifying the dissolution behavior of SEI components in various $NaPF_6$-based carbonate electrolytes, binary solvents such as EC:DEC were found to promote the formation of more stable, less soluble SEI layers and reduce interfacial degradation—particularly when supplemented with inorganic additives like NaF.[202] Ether-based electrolytes offer lower viscosity and high ionic conductivity and have demonstrated favorable interfacial behavior with alloy anodes.[203,204] For example, Sn electrodes cycled in 1.0 M $NaPF_6$ in dimethoxyethane (DME) electrolyte exhibited enhanced cycling stability due to the unique solvation structure of the ether solvent.[200] However, this stability is highly sensitive to the solvent or salt composition. Ether electrolytes have been demonstrated to stabilize the micro-sized Sn anode by forming a robust connection to the organic matrix, which renders superb mechanical properties.[205] Sulfone-based electrolytes (such as dimethyl sulfoxide (DMSO), tetramethylsilane (TMS)) provide good thermal and electrochemical stability, and their high dielectric constant supports better salt dissolution.[206–208] Yet, their high viscosity can impair rate performance. Moreover, their strong polarity affects SEI composition and may require co-optimization with additives[209] or surface coatings. Strategies such as localized high-concentration electrolytes may help reconcile these trade-offs.[210] Electrolyte optimization for alloy anodes must balance SEI stability, ionic conductivity, and chemical compatibility.

[H3] Binder engineering

Functional polymeric binders play a crucial role in accommodating volume changes for battery electrodes during cycling, especially in alloy anodes like Si (for LIBs), phosphorus, and tin, which undergo expansions exceeding 400% upon charge-discharge process.[211,212] In LIBs, polyacrylic acid and carboxymethyl cellulose improve electrode cohesion by forming hydrogen bonds or crosslinked networks with the active materials.[213,214] These binders enhance mechanical integrity, suppress electrode cracking, and maintain electronic connectivity throughout repeated cycling. The mechanical properties of the binder, especially elasticity, tensile strength, and ductility, are the keys to managing dimensional changes without structural failure.

Similar design strategies are being extended to sodium-ion systems. Hybrid binders that integrate hydrogen-bonding motifs and flexible architectures are being developed to maintain a stable conductive network (Figure 4e).[215] Additionally, binder–electrolyte compatibility must be optimized to prevent dissolution and ensure chemical stability.[216] Recent advances include crosslinked polymer systems (such as PPA–glycerin[217]), which substantially improve the mechanical properties and cycling life of micro-structured Sn electrodes. Ultimately, the ideal binder must balance mechanical flexibility, chemical resistance, and adhesion strength to maintain high performance over extended cycles.

[H3] Gel-polymer electrolytes

Gel-polymer electrolytes have emerged as a multifunctional platform to simultaneously address mechanical instability, interfacial degradation and safety in alloy-type anodes.[218,219] Drawing from LIB research, these electrolytes integrate ion conduction with mechanical reinforcement by embedding sodium salts and plasticizers into polymer matrices such as poly(vinylidene fluoride-hexafluoropropylene), poly(ethylene oxide), or similar polymers (Figure 4f).[220,221] These can be cured in situ with photon or thermal processes, allowing intimate contact with active materials and eliminating interfacial voids.

The performance of gel-polymer electrolytes in NIBs can be systematically tuned by engineering multiple structural and compositional parameters.[222,223] Crosslinking density within the polymer matrix governs the trade-off between mechanical robustness and ionic conductivity.[224] Although higher crosslink densities enhance structural integrity and resistance to volume fluctuations, excessively rigid networks can impede Na^+ mobility. The choice and proportion of plasticizers—typically organic solvents such as EC, PC, or ionic liquids—strongly influence viscosity, ionic mobility, and gel flexibility. An optimal balance must be achieved to maintain both conductivity and mechanical adaptability. Salt types and concentration are critical to the electrolyte's conductivity. High salt loading can increase viscosity and hinder ion dissociation, whereas low concentrations result in insufficient charge carriers and reduced ionic transport. Gel thickness and residual solvent content directly affect

cell-level energy density and interfacial resistance. A thinner, well-integrated gel layer minimizes ion transport barriers while ensuring conformal contact with electrode surfaces. Finally, the incorporation of functional additives or secondary nanofillers—such as ceramic nanoparticles or inorganic reinforcements—can further enhance the mechanical modulus, thermal stability, and interfacial compatibility of gel-polymer electrolytes. These nanostructured fillers act as structural anchors, suppress polymer chain mobility, and reinforce the gel–electrode interface.[225,226] Through the rational tuning of these parameters, in situ-formed gel-polymer electrolytes can offer both mechanical support and efficient Na^+ transport, effectively mitigating the severe stress and interfacial instability that plague alloy-type anodes in NIBs.

[H3] Composite electrode strategy

Hybrid or multi-component electrodes, such as HC–phosphorus,[150,227,228] HC–tin,[157,160,193,229] and phosphorus–tin[209,230,231] composites, are promising architectures for addressing the intrinsic limitations of alloy-type anodes in NIBs. These designs aim to mitigate critical issues that frequently affect single-component alloy systems, such as large volume changes, low electrical conductivity, and unstable electrode–electrolyte interfaces. Recent findings further demonstrate that inactive components such as Si, when incorporated into multi-metallic composites, can effectively buffer internal stress and enhance structural reversibility, even though they may not directly contribute to capacity.[232]

Core to this approach is the structural integration of HC or secondary alloy phases, which buffer volume expansion, enhance conductivity, and improve mechanical resilience.[150,233] Likewise, combining two alloy materials such as P and Sn allows for stress distribution across distinct alloying phases, smoothing of large volume transitions, and tuning of the sodiation potential range.[234,235] These composite structures frequently leverage the mechanical support of the matrix and the electrochemical reactivity of the active phases to achieve improved cycling stability and capacity retention. However, hybrid electrodes also introduce new challenges. Interfaces between different components must be carefully engineered to avoid

delamination and extra interfacial impedance. Moreover, the mass ratio between active material and matrix require precise control: excessive carbon content can dilute energy density, while insufficient matrix support may fail to buffer structural degradation.[193,236,237] Scalable synthesis techniques with tunable nanoscale or microscale architecture remain essential for translating these designs to practical use.

Importantly, many hybrid systems demonstrate synergistic effects that extend beyond simple additive contributions. For example, C–Sn composites benefit not only from the conductivity of carbon but also from its ability to suppress Sn nanoparticle agglomeration.[233] Similarly, P–Sn composites allow for phase-distributed alloying reactions that mitigate mechanical fracture by distributing the strain across multiple alloying steps.[230] To maximize these effects, rational design must integrate structural, chemical, and electrochemical optimization. From a materials perspective, control over the dispersion and size of alloy domains in core–shell configurations, porous networks, or hierarchical scaffolds can accommodate dimensional changes while maintaining electronic percolation. Electrochemically, tuning the potential window and reaction kinetics of each component is critical. For example, balancing the reactivity of P and Sn within a shared matrix requires careful adjustment of composition, phase distribution, and voltage overlap.[238]

By unifying structural reinforcement, interface stabilization, and electrochemical tuning, multi-phase composite electrodes such as C–P, C–Sn, and P–Sn are a powerful strategy to overcome the trade-offs of conventional alloy anodes. Future developments will hinge on a system-level understanding of materials chemistry, device engineering, and manufacturing, each part essential to unlocking the full potential of alloy-based NIBs.

[H1] Frontiers in Manufacturing

[H2] Electrode engineering for high areal capacity

Achieving high areal capacities, progressing from 3 mAh cm^{-2} toward 6 mAh cm^{-2} and beyond, is a critical benchmark for next-generation batteries.[239–241] Both HC and alloy-based anodes present distinct opportunities and engineering challenges when transitioning to thick-film

electrodes.

Alloy-type anodes such as red or black P, Sn, and Pb offer substantially higher specific capacities than HC, such as up to 2000 mAh g^{-1} for red P,[150] allowing target areal capacities to be reached with much lower active mass (for example, ~3 mg cm^{-2} for 6 mAh cm^{-2}). In contrast, HC may require > 20 mg cm^{-2} to achieve the same capacity. Despite this advantage, alloy materials face critical limitations related to extreme volume expansion during (de-)sodiation. These dimensional fluctuations, when magnified in thicker electrodes, intensify internal mechanical stress, resulting in accelerated particle fracture, delamination, and electrical disconnection. Moreover, non-uniform sodiation kinetics across thick layers can exacerbate strain gradients and trigger early-stage electrode degradation. As a result, achieving 3 mAh cm^{-2} or more with alloy materials demands comprehensive electrode-engineering solutions.

To enable alloy anodes to operate at high areal capacities, solutions must go beyond material-level design and extend to electrode-level engineering.[242] A key strategy involves constructing hierarchical electrode architectures that can buffer global stress accumulation and enhance ion/electron transport across the entire electrode thickness. For example, introducing graded porosity or aligned pore channels enables efficient Na^+ penetration, reducing internal concentration gradients and ensuring uniform electrochemical activity. These structural features help avoid strain localization, particularly near the current collector or electrode surface.[243,244] In parallel, electrode formulation parameters—including the distribution of active material, binder, and conductive additives—must be systematically optimized to maintain electronic percolation and mechanical integrity under repeated cycling.[241,244,245] Specifically, thicker alloy-based electrodes require binders with enhanced elasticity and interparticle adhesion, not only to buffer local expansion but also to preserve cohesive stress transfer throughout the electrode matrix. In high-loading designs, electrolyte access and retention become equally critical. Tailoring the electrolyte composition and viscosity, or adopting electrolyte-gel integration, can facilitate deeper infiltration and reduce dry zones in thick electrodes.

As NIB technology moves toward thicker electrodes and higher areal capacities, both HC and alloy-type anodes must surmount limitations in ionic and electronic transport, mechanical resilience, and SEI stability. The path forward relies on integrated strategies: advanced electrode architectures that balance density with access to electrolyte, robust binders or coatings that withstand repeated volume changes, and possibly electrolyte innovations that form more stable interfaces under high loading. By simultaneously addressing these factors, researchers can pursue high areal capacities while preserving cycle life and rate performance.

[H2] Presodiation

The loss of active sodium due to irreversible side reactions substantially reduces both the ICE and reversible capacity of sodium-ion full cells. Pre-sodiation has emerged as an effective strategy to mitigate this issue and improve the areal capacity.[30,246,247] However, several challenges must be overcome before its practical implementation. First, the pre-sodiation agent should decompose sufficiently during formation to release active sodium while minimizing the formation of inactive residues that may lower cell energy density. Second, it is preferable for the pre-sodiation agents to be reasonably stable in ambient air to enable safe handling and integration into current manufacturing processes. Finally, the agent should ideally be chemically compatible with existing electrode and electrolyte chemistries, minimizing the risk of unwanted side reactions. Meeting all these requirements simultaneously remains highly challenging. Current pre-sodiation approaches can be broadly categorized into two main types: use of electrochemically decomposable salts and foreign electrode materials, and over-sodiation of electrode materials.

Electrochemically decomposable salts such as NaN_3[248], Na_2CO_3[249], $NaNO_2$[250], $Na_2C_4O_4$[251], $Na_2C_2O_4$[252], and NaAc[253] are typically incorporated into the electrode slurry and decompose during the initial formation cycles to release Na^+ and gaseous byproducts, leaving no residual solids. For instance, di-sodium squarate ($Na_2C_4O_4$) was synthesized as a new environmentally benign and cost-effective sodium salt and incorporated into the $Na_3(VO)_2(PO_4)_2F$ cathode during slurry preparation.[251] The decomposition of $Na_2C_4O_4$ at 3.6 V generates CO_2, which is released after cell formation. This process increases electrode

porosity, enhancing ion transport and improving material utilization and capacity, particularly at higher rates. Use of these salts is not without limitations, however. First, decomposition may be incomplete, leaving behind residual solids that increase internal resistance or interfere with SEI formation. Second, gas evolution can cause porosity gradients or delamination in thick electrodes, particularly at high loadings. Third, the electrochemical window required for full decomposition may not align with standard formation protocols, leading to process complexity.

Foreign electrode materials such as $NaCrO_2$[254], Na_3P[255], and Na[256–258] can also serve as pre-sodiation agents. Na_3P, when added to $Na[Fe_{0.5}Mn_{0.5}]O_2$, compensates for SEI-related sodium loss and produces elemental phosphorus, which acts as a safety buffer during over-discharge[255]. Additionally, introducing metallic sodium, either through thermal decomposition of $NaBH_4$[258] or vacuum thermal evaporation[256], promotes the formation of a thin SEI on HC, leading to increased initial CE and higher energy density. However, these agents often require careful control over their redox activity to avoid over-compensation, which may reduce ICE or compromise long-term cycling. Air and moisture sensitivity is another concern, which makes them generally not compatible with high-throughput electrode fabrication.

Another effective strategy is over-sodiation, which stores excess Na^+ within multivalent electrode materials to offset initial sodium loss. This approach requires a transition metal center capable of multiple valence states. In one successful example, $Na_3V_2(PO_4)_3$ was electrochemically converted to $Na_4V_2(PO_4)_3$ and paired with a HC anode[259]. The resulting full cells exhibited a 76% increase in energy density. Besides electrochemical over-sodiation, chemical over-sodiation using Na^+-rich solutions like Na-naphthalene in tetrahydropyran has also been demonstrated with $Na_{0.67}Fe_{0.1}Al_{0.1}Mn_{0.8}O_2$ cathode[260], providing a scalable and cost-effective pre-sodiation route for practical battery manufacturing. For this route, ensuring uniform Na^+ distribution and avoiding unwanted reactions with binder or surface impurities remain practical challenges.

Beyond compensating for initial sodium loss, the pre-sodiation process can potentially improve SEI quality and electronic conductivity of the electrode. For example, sodium bis(2-methoxyethoxy) aluminum hydride has been used as a pre-sodiation reagent in HC anodes[261].

Its decomposition not only compensates for sodium loss but also forms a passivating Al_2O_3 nanolayer, which suppresses electrolyte decomposition, improves air stability, and enhances capacity and retention in full cells.

A further important consideration is placement strategy. Most of the salt sacrifices are often embedded into the cathode, where oxidative potential can trigger their decomposition efficiently and allow Na^+ to diffuse to the anode via the electrolyte. However, for HC or alloy-based anodes with high irreversible Na consumption, direct integration into the anode side could ensure more localized Na delivery and minimize parasitic crosstalk. Yet, this approach poses greater challenges in handling air-sensitive agents and controlling uniform dispersion. Therefore, cathode-side integration is generally more practical and scalable, whereas anode-side approaches may be more suitable for specialized designs or pouch cell preconditioning.

In summary, although presodiation has proven effective in improving ICE and energy density, each strategy presents trade-offs in decomposition efficiency and processing compatibility. Moving forward, the rational design of presodiation systems will require application-specific balancing between several critical factors, including efficiency, stability, and manufacturability.

[H1] Characterization

Understanding the complex reaction mechanisms of high-performance anodes demands a comprehensive suite of characterization that spans multiple length scales, ranging from atomic-level interactions to cell behavior (Figure 5). Here, we highlight key techniques in four domains: synchrotron-based operando methods, interface analysis, atomic and local structural characterization, and gas evolution characterizations, while critically assessing their capabilities and limitations.

[H2] Synchrotron characterization

Synchrotron tools are extremely powerful for elucidating the structural and chemical transformations of anode materials during electrochemical cycling.[18,150,187] X-ray absorption spectroscopy (XAS) provides insights into the oxidation states and local coordination during

complex redox behavior in alloy-type anodes. For example, operando Sn K-edge XAS has revealed the sequential transformation from Sn^0 to $Na_{15}Sn_4$ and back, capturing subtle redox reversibility and alloying hysteresis during cycling[262,263]. Similarly, P K-edge XAS has been used to probe the decomposition of Na_3P and formation of intermediate phases, providing critical insights into irreversible capacity loss mechanisms.[264–266]

For HC anodes, which are largely amorphous and turbostratic, pair distribution function (PDF) analysis is particularly useful. It enables quantitative characterization of short-range order and graphitic domain correlation lengths, offering structural descriptors that correlate with slope and plateau capacities. Besides ordering, pore identification is critical. Small-angle neutron scattering (SANS) and SAXS have proven indispensable, both at the surface and within the bulk of HCs for characterization of closed pores, which are inaccessible to gas probes.[53,267–269] Notably, operando SAXS can monitor the evolution of porosity during sodiation/desodiation processes, thereby offering dynamic insights into structural changes under realistic cycling conditions.[268] When combined with wide-angle X-ray scattering (WAXS), a more comprehensive picture of both short- and long-range order in HC can be obtained.[53,269–271]

X-ray computed tomography (XCT) enables three-dimensional visualization of electrode microstructure, capturing crack formation, pore development, and binder–particle interactions across charge–discharge cycles.[272–274] Advanced methods such as phase-contrast XCT reveal even low-density regions like voids or early delamination zones from low-Z materials such as carbon. At finer spatial scales, transmission X-ray microscopy (TXM) offers sub-40 nm resolution, combining spatial mapping with chemical sensitivity to reveal the distribution of redox-active phases or oxidation states across the electrode.[20,275,276] Such chemical imaging is particularly beneficial for multi-phase alloy composites or HC materials infused with additives.[277,278] For example, in situ X-ray nanotomography and TXM have been utilized to visualize the 3D (de-)sodiation of Sn anodes, revealing unexpected structural and morphological reversibility during the 1st cycle.[279] For resolution finer than what is capable from X-ray optics, ptychography provides sub-probe resolution with scanning TXM.[280] For even deeper insight, Bragg coherent diffraction imaging (BCDI) can detect nanoscale strain

fields within single grains, revealing how local mechanical stress correlates with degradation pathways.[281,282]

Depth-resolved characterization techniques, including nano-/micro-focused X-ray diffraction (XRD), XAS, and X-ray fluorescence (XRF) mapping, as well as grazing incidence diffraction, have considerable potential to probe vertical heterogeneity in thick electrodes. Despite their powerful capabilities, many of these advanced synchrotron imaging techniques, particularly ptychography and BCDI, remain underutilized in the study of NIB anodes due to their experimental complexity, limited beamline accessibility, and stringent requirements for sample geometry and cell design. In practice, the application of such frontier tools to NIB systems is still emerging. This is particularly evident for hard carbon anodes, where the intricate and spatially heterogeneous Na^+ storage mechanisms pose major challenges for spatially resolved operando analysis. Similarly, alloy-type anodes suffer from substantial volume and strain changes and interface reconstruction during cycling, yet the lack of high-resolution, time-resolved structural data has hampered mechanistic understanding of their degradation pathways. Broadening the application of cutting-edge synchrotron techniques to NIB anodes would not only offer transformative insights into fundamental electrochemical processes but also support more informed materials design and engineering. Furthermore, the unique structural dynamics of NIB systems, such as the open/closed pore behavior of HC or the metastable intermediate phases in alloy composites, may in turn drive new developments in synchrotron science itself, stimulating the advancement of multimodal, high-throughput, and more accessible characterization platforms.

[H2] Interface characterization

The formation and stability of the SEI are pivotal for long-term anode performance. Surface-sensitive techniques such as nanoscale Fourier Transform infrared spectroscopy (nano-FTIR) and spectroscopic ellipsometry offer detailed insights into interfacial chemical compositions and dynamics.

Nano-FTIR is an analytical technique that utilizes a sharp metallic atomic force microscopy (AFM) probe to focus infrared (IR) light at the tip apex, generating a highly

localized near-field interaction with the sample (Figure 5b).[283–285] The scattered near-field IR signal yields spectra with spatial resolution on the order of ~20 nm, which is two orders of magnitude finer than conventional IR microscopy (2–5 μm). Given the powerful sensitivity of IR spectroscopy to both organic and inorganic compounds, nano-FTIR has proven highly effective in a variety of applications.[286] In the last 2-3 years, this technique has been applied to probe the SEI on LIB anodes under both ex situ and in situ configurations.[287–291] Results reveal nuanced variations in SEI composition and structure across different surfaces and electrolyte chemistries, particularly in terms of organic/inorganic content and chemical homogeneity. For sodium-ion systems, synchrotron-based IR nano-spectroscopy offers additional advantages due to its extended detection range into the far-IR (down to ~200 cm^{-1}), enabling the identification of Na-based inorganic SEI components such as NaF and Na_2O.[291–293] Given the importance of these species in stabilizing alloy-type and HC anodes, nano-FTIR is poised to become a critical tool for unraveling the relationship between SEI nanostructure and electrode-electrolyte configurations in Na-ion batteries.

Spectroscopic ellipsometry is an optical technique that measures changes in the polarization of light reflected from a surface at oblique angles (Figure 5c). By modeling the polarization response based on known optical constants, this technique can quantitatively resolve the thickness and refractive index of thin surface layers with exceptional sensitivity. Commonly used in semiconductor metrology, ellipsometry has also been employed to track SEI formation on battery anodes—notably on model surfaces such as specific facets of Sn single crystals, highly oriented pyrolytic graphite, and amorphous Si films.[294–296] In situ ellipsometry offers temporal resolution on the order of sub-seconds, enabling researchers to directly correlate electrochemical cycling with the dynamic evolution of interfacial films. This capability is particularly relevant for Na-ion alloy anodes like Sn, where electrolyte reduction products are often soluble, preventing robust SEI formation.[297] By monitoring changes in film thickness or refractive index, ellipsometry can reveal whether SEI components precipitate and adhere to the surface or dissolve into the electrolyte, offering insight into passivation mechanisms. These observations are invaluable for guiding electrolyte formulation and

interface engineering to improve SEI stability on sodium-alloy anodes.

[H2] Atomic and local structural characterization

Conventional techniques such as XRD[298] and neutron scattering,[46] combined with PDF analysis, have been widely used to probe the local structural arrangement and crystallinity of HCs. However, due to the intrinsic structural heterogeneity of HC, these values are statistical averages and do not reflect local structural variations. Microporosity in HCs—typically classified as open versus closed pores—also plays a pivotal role in sodium storage, particularly through nanopore-filling processes. Open pores can be effectively characterized using gas adsorption/desorption isotherms.[299] The choice of probe gas (such as N_2, CO_2, He) must be carefully selected based on molecular diameter and accessibility, as different gases may preferentially enter distinct pore types.

High-resolution transmission electron microscopy (TEM) remains one of the few techniques capable of simultaneously imaging *d*-spacing and microstructure[91]. It is important to note that TEM and diffraction techniques can provide only local or averaged *d*-spacing values due to the highly disordered carbon layer arrangement in hard carbon, making it difficult to define a fixed value. In contrast, 3D electron tomography (ET) has emerged as a powerful tool for visualizing the three-dimensional architecture of electrode materials[300], including HC,[301] offering more representative insights into structural features that are inaccessible through conventional 2D imaging. Furthermore, sodium's high reactivity in ambient conditions poses a considerable challenge for observing sodiation states using conventional microscopy. In this context, Cryo-EM or Cryo-ET (Figure 5a) has emerged as a powerful method for visualizing battery materials in their native states.[300,302] By rapidly freezing samples at specific states of charge (for example, -176 °C), Cryo-EM and Cryo-ET preserve delicate microstructures and minimize beam-induced damage, thus enabling accurate imaging of sodium storage behavior and interfacial evolution in HCs and alloy anodes during cycling.

High-resolution TEM is indispensable for probing the nanoscale architecture of alloy-based anodes, especially crystal domain boundaries, lattice distortions, and heterointerfaces in composite structures. For instance, TEM imaging of Sn–C and SnSb–C composites reveals

well-defined phase separation and intimate carbon–metal contact, which are crucial for accommodating stress and enhancing electronic connectivity[179]. Moreover, advanced contrast techniques, such as high-angle annular dark-field scanning transmission electron microscopy (HAADF-STEM) and electron energy loss spectroscopy (EELS), allow mapping of elemental distributions and oxidation states across interfaces, revealing the degree of compositional homogeneity and potential SEI–bulk interactions. Such capabilities are especially important for evaluating the structural integrity and interfacial chemistry of nanostructured alloy anodes after extended cycling, where mechanical degradation often initiates at invisible heterointerfaces.

In situ TEM has become a vital tool for capturing the real-time structural evolution of alloy and composite anodes during (de-)sodiation. For instance, β-SnSb was shown to undergo a well-defined two-step sodiation pathway involving the formation of Na_3Sb and $Na_{15}Sn_4$ intermediates, which subsequently revert to the original β-SnSb phase upon desodiation[303]. Similarly, Ge-based nanowires display distinct behaviors depending on their initial structure: whereas crystalline Ge exhibits sluggish sodiation, amorphized Ge enables rapid and homogeneous Na insertion with over 300% volume expansion, forming nanopores and crack fronts that evolve with cycling.[304] These insights underscore the importance of understanding how different alloy chemistries and structural motifs interact with sodium at the nanoscale.

Solid-state NMR (ssNMR) can elucidate sodium storage mechanisms and interfacial chemistry in both hard carbon (HC) and alloy-based anodes. For HC, ssNMR enables the differentiation of Na ions stored between disordered graphene layers and those confined in nanopores, revealing that sodium resides in distinct, non-metallic environments and exhibits sluggish site exchange kinetics[54]. Other advances have applied ssNMR to probe the evolution of solid electrolyte interphase (SEI) layers during cycling, identifying sodium-containing species such as NaF, Na_2CO_3, $NaBF_4$, and sodium borates formed from additive decomposition[305,306]. Moreover, operando and multidimensional NMR approaches have been employed to monitor real-time sodium dynamics and provide site-specific insights into Na coordination environments, which are essential for optimizing capacity retention, improving

ICE, and designing robust SEI chemistries.[307,308]

[H2] Gas evolution characterization

Gas evolution is both a critical safety concern and a sensitive marker of parasitic reactions in NIBs, reflecting electrolyte decomposition, interphase instability, and irreversible sodium loss that collectively undermine battery health. Real-time gas analysis tools are key to dissecting these processes and include differential electrochemical mass spectrometry (DEMS) and online electrochemical mass spectrometry (OEMS), which track the identity and rate of gases such as H_2, CO_2, CH_4, or even toxic cyanogen.[309–311] Complementary methods such as titration mass spectrometry (TMS), in situ pressure monitoring, and ultrasonic scanning imaging provide bulk and surface gas accumulation and release mechanisms over long cycling.[312]

The anode fundamentally dictates whether and how gases form, whose potential window controls whether electrolyte reduction produces stable SEI components or gaseous fragments. In turn, gas evolution directly governs anode performance. Persistent gas generation consumes electrolyte and cyclable sodium, drives SEI rupture and reformation, and increases impedance. For example, DEMS measurement reveal the generated CO_2 and H_2 in Sn foil continually rupture the nascent SEI, whereas metallurgical pre-alloying of Sn with Na lowers its open-circuit potential and markedly suppresses gassing, tripling initial Coulombic efficiency.[313] Joint in situ Ultrasonic scanning and DEMS measurement demonstrate HC exhibits a distinct gas behavior. Its nanoporous structure adsorbs gases generated during charging, which then desorb in the first discharge, causing unexpected gas release patterns.[311] Even sodium metal itself is sensitive: a combined operando TEM, operando AFM, and DEMS research show that when paired with carbonate electrolytes, it promotes intensive bubble formation, but in ether systems, a softer, more elastic SEI conforms to the electrode surface and suppresses gas evolution.[314]

Collectively, these findings establish gas evolution analysis not merely as a diagnostic tool but as a mechanistic bridge between anode–electrolyte reactions and the practical stability and safety of SIBs.

[H1] Perspective

The development of next-generation sodium-ion battery anodes is now at an inflection point: the field has moved beyond proof-of-concept discoveries and must confront the realities of performance targets, manufacturing, and system integration. HC and alloy-type materials, the two pillars of NIB anode research, each offer complementary advantages, but also carry distinct bottlenecks that must be strategically addressed. Below, we outline four priority directions that should guide research and industrial efforts in the coming decade.

[H2] Mechanism-driven design of hard carbons

HC will remain the baseline anode for commercial NIBs, but its further advancement hinges on transforming today's largely empirical synthesis into a mechanism-driven science. Fundamental questions, such as the relative contributions of adsorption, interlayer insertion, and nanopore filling, or the chemical state of stored Na, remain unresolved. Multimodal operando tools (such as SAXS/WAXS coupling, cryo-EM, ssNMR) should be deployed not merely to "observe" but to build predictive structure–capacity models. Such models would enable rational tailoring of spacings, pore topology, and surface chemistry to simultaneously achieve ≥ 450 mAh g^{-1} specific capacity, high ICE, and long-term cycling stability.

[H2] Engineering alloy-type anodes from nano to practical scale

Alloy anodes, especially Sn and P, promise transformative energy density gains. To realize these gains, a pivot from nanoscale to micron-scale architectures and thick-electrode designs that reconcile volumetric expansion with manufacturability will be key. This entail hierarchical structures that buffer stress across scales; elastic binders and gel polymer electrolytes to sustain mechanical integrity; and processing routes such as spray drying and scalable carbon coating that are compatible with ton-scale production. The focus should shift from "maximum capacity" to "capacity retention under realistic areal loading."

[H2] System-level integration beyond the anode itself

Future progress will not come from isolated anode optimization. Electrolyte formulation,

SEI design, and pre-sodiation strategies must be co-engineered with HC and alloy materials. For example, high-capacity alloys require SEIs that are elastic yet chemically robust, whereas HC benefits from pre-sodiation schemes that improve ICE without creating porosity gradients. These interactions should be mapped in a "design matrix" framework—linking material type, electrolyte chemistry, and processing sequence—to guide tailored solutions for different cell chemistries (for example, grid-scale vs. high-power NIBs).

[H2] Scalability, sustainability, and supply-chain readiness

Finally, any anode innovation must pass the industrial feasibility filter. Biomass-derived HCs face compositional variability; alloy anodes like Sb or Bi are limited by elemental scarcity; even promising candidates like red P raise safety and handling issues. The field must identify "manufacturing anchors", precursors, synthesis protocols, and composite designs that are inherently scalable, safe, and cost-competitive. Close collaboration between academia, industry, and policy makers will be critical to translate lab-scale breakthroughs into supply-chain-secure, gigawatt-hour-ready solutions.

Looking forward, the future of NIB anodes will not be defined by a single "miracle material," but by converging innovations across materials science, electrochemistry, and engineering. By shifting focus toward mechanism-informed HC design, engineering alloy anodes for industrial conditions, and embedding these materials into fully integrated battery systems, the NIB community can deliver anode technologies that are not just high-performing in the lab, but truly transformative in industry.

Acknowledgements:

This work was supported by the Office of Vehicle Technologies of the U.S. Department of Energy through the Advanced Battery Materials Research (BMR) Program (LENS Consortium).

Author Contributions: G.-L.X., W.Z., Y.C., V.S. and K.A. envisioned and developed the review. W.Z and Z.L. contributed equally to this work. W.Z. and Z.L. carried out the literature

survey, analyzed the data, and prepared the figures. All authors contributed to the discussion and writing of manuscript.

Competing interests: All the authors declare no competing interests.

Data availability

All data are available in the main text.

Display items

Table 1. Structural features and representative electrochemical properties of alloy anodes for NIBs

Chemical	Structure				Electrochemistry					Scalability
	Space group	Coordination	Bonding Type	Structural types	Sodiation phase	Theoretical capacity (mAh g^{-1})	Specific capacity (mAh g^{-1})	Volume expansion	Ref.	
Si	Amorphous	≈ 4 (Si-Si sp^3)	Strong covalent	3D disordered	$Na_{0.76}Si$	725	340	114%	[144]	Low
Red P	Amorphous	≈ 3	Random P-P chains	Disordered	Na_3P	2596	2481	308%	[227,315,316]	High
Black P	C222	3	Covalent chains	1D chains	Na_3P	2596	2206	~ 400%	[150]	Low
Sn	$I4\bar{1}/amd$	6	Distorted metallic	3D framework	$Na_{3.89}Sn$	878	860	451%	[155,157,158]	Moderate
					$Na_{3.75}Sn$	847	878	424%	[142]	
Sb	$R\bar{3}m$	6 (3 strong + 3 weak)	3 covalent + 3 weak	Pseudo-layered	Na_3Sb	660	624	390%	[317,318]	Low
Ge	$Fm\bar{3}m$	4	Strong covalent	3D framework	$Na_{1.56}Ge$	576	590	205%	[155]	Low
Pb	$Fm\bar{3}m$	12	Metallic	3D framework	$Na_{15}Pb_4$	485	475	386.9%	[165]	Moderate

Bi	$R\bar{3}m$	6 (3 strong + 3 weak)	3 covalent + 3 weak	Pseudo-layered	Na_3Bi	385	~380	~ 250%	[168,319]	Low

Figure 1 | Commercialization status and performance outlook of high-energy NIBs. a. Global landscape of sodium-ion battery (NIB) commercialization, highlighting large industrial companies (yellow), major national-scale projects (red), and grid-scale deployments (blue). **b.** Projected improvements in full-cell energy metrics for NIBs via alloy-type anode design. Specific and volumetric energy densities are plotted for Sn- and P-based composites at varying contents, benchmarked against current HC–NFM333 ($NaNi_{0.33}Fe_{0.33}Mn_{0.33}O_2$, using a fixed specific capacity of 125 mAh g^{-1}) cells. The orange shaded region highlights the typical performance window of commercial LFP/graphite LIBs, underscoring the competitiveness of optimized NIB systems. Data source: LENS, U.S. Department of Energy.

Figure 2 | Design strategies for high-capacity HC anodes. Optimizing precursor selection, synthesis protocols, and structural design enhance electrochemical performance and scalability of HC for practical NIB applications. **a.** HCs have complex structural properties, including nano- and micro-sized porosity, amorphous domains, and turbostratic carbon layers,which lead to distinct electrochemical performances. **b.** Surface functionalization, heteroatom doping, and nanoparticle embedding can expand the interlayer distance and introduce defects, improving sodium insertion and plateau capacity. **c.** A wide range of precursors, including biomass, synthetic polymers, and fossil carbon sources, are used to tailor the microstructure through thermal treatment, affecting pore architecture and crystallinity. **d.** Engineering of carbon interlayers and pore morphology, such as regulating d-spacing and closed pore size, offers opportunities to boost both sloping and plateau capacities. **e.** Timeline of reported advanced HCs with ultrahigh capacity. [a]: ref.[128], [b]: ref.[107], [c]: ref.[109], [d]: ref.[91], [e]: ref.[115], [f]: ref.[59], [g]: ref.[111], [h]: ref.[75], [i] ref.[126], [j] ref.[127], [k] ref. [121]

Figure 3 | Structural characteristics, natural abundance, and annual production of representative anodes for NIBs. a–h) Schematic illustrations of **a.** HC, **b**. red P, **c**. black P, **d.** Ge, **e.** Sn, **f.** Pb, **g.** Sb, and **h.** Bi, with applicable space groups indicated. HC consists of disordered graphene-like layers with curved, turbostratic stacking. Red P has an amorphous polymeric network, while black P adopts a puckered layered structure. Alloy-type anode elements including Ge, Sn, Sb, Pb, and Bi exhibit diverse crystal symmetries, suggesting variable bonding environments and potential phase transformation pathways upon sodiation. **i.** Schematic comparison of natural abundance (in ppm) of the alloy elements, illustrating a wide disparity ranging from trace Bi (0.0085 ppm) to abundant P (~1000 ppm). **j.** Estimated global production per year (in tons), visualized by scaled transport truck icons. Production spans over six orders of magnitude, from 155 t/year (Ge) to ~2.3×10^8 t/year (P), highlighting the potential availability constraints of certain alloying-type elements in large-scale NIB deployment. Data source for c-h: ICSD[172] and The Materials Project[173]. Data source for i and j: Wikipedia[180].

Figure 4| Structural design strategies for alloy-based anodes. a. The large volume change and mechanical instability of alloy-type anodes during sodiation/desodiation cycles leads to severe pulverization and cracking, posing major challenges for practical application. **b.** Nano-engineered architectures, including nanodots, nanoarrays, nanowires, and core–shell structures, shorten Na^+ diffusion lengths and improve mechanical resilience. **c.** Carbon composite strategies embed nanoscale alloy particles within carbon matrices, improving electrical conductivity, buffering volume expansion, and stabilizing the electrode–electrolyte interface. **d.** Micro-engineering integrates micro-/nano-domains within a mechanically robust framework and introduces dopants to enhance durability, structural stability, and cycling performance under practical electrode conditions. **e.** Hybrid binder systems employ dual polymer components to form hydrogen-bonded and crosslinked networks around alloy particles, enhancing elasticity, mechanical adhesion, and crack resistance. **f.** Gel-polymer electrolytes consist of sodium salts and plasticizers embedded within polymer matrices that conformally coat alloy particles, promoting homogeneous ion transport and buffering interfacial stress.

Figure 5 | Multi-scale strategies for characterizing interfacial and bulk evolution in NIB anodes. a. Cryo-EM preserves the native state of sodium-containing interfaces, enabling direct nanoscale imaging of SEI and microstructural changes during cycling. **b.** Nano-FTIR enables nanoscale-resolved chemical information of SEI layers by combining incident IR excitation with detection via an AFM probe. **c.** Spectroscopic ellipsometry monitors real-time changes in SEI layers by analyzing the polarization of reflected light, providing sub-nano sensitivity during SEI evolution. **d.** NMR probes local chemical environments in solid or liquid phases, yielding information on ion coordination and mobility in electrode and electrolyte systems. **e**. Synchrotron-based characterizations enable *in situ* chemical, structural, and morphological analysis. Combining these techniques provides comprehensive surface and bulk insights into dynamic chemical and structural evolutions during electrochemical operation.

References

1. Yabuuchi, N., Kubota, K., Dahbi, M. & Komaba, S. Research development on sodium-ion batteries. *Chem. Rev.* **114**, 11636–11682 (2014).

2. Vaalma, C., Buchholz, D., Weil, M. & Passerini, S. A cost and resource analysis of sodium-ion batteries. *Nat. Rev. Mater.* **3**, 18013 (2018).

3. Usiskin, R. *et al.* Fundamentals, status and promise of sodium-based batteries. *Nat Rev Mater* **6**, 1020–1035 (2021).

4. Zuo, W. & Yang, Y. Synthesis, Structure, Electrochemical Mechanisms, and Atmospheric Stability of Mn-Based Layered Oxide Cathodes for Sodium Ion Batteries. *Acc. Mater. Res.* **3**, 709–720 (2022).

5. Zuo, W. *et al.* The stability of P2-layered sodium transition metal oxides in ambient atmospheres. *Nature communications* **11**, 3544 (2020).

6. Yang, Y. *et al.* Decoupling the air sensitivity of Na-layered oxides. *Science* **385**, 744–752 (2024).

7. 钠离子电池发布会. https://www.catl.com/technologybrand/6251.html?utm_source=chatgpt.com.

8. Naxtra Battery Breakthrough & Dual-Power Architecture: CATL Pioneers the Multi-Power Era. https://www.catl.com/en/news/6401.html.

9. 中科海钠科技有限责任公司. https://www.hinabattery.com/.

10. Technology Benefits. *Faradion* https://faradion.co.uk/technology-benefits/.

11. Why TIAMAT. *TIAMAT* https://www.tiamat-energy.com/.

12. Zhang, P. China's 1st large-scale sodium battery energy storage station put into operation. *CnEVPost* https://cnevpost.com/2024/05/13/china-1st-large-sodium-battery-energy-storage-station-operation/ (2024).

13. Zhang, P. 'World's largest' sodium-ion battery energy storage project goes into operation in China. *CnEVPost* https://cnevpost.com/2024/07/02/world-largest-sodium-battery-energy-storage-project-in-operation/ (2024).

14. Zhu, Z. *et al.* Rechargeable Batteries for Grid Scale Energy Storage. *Chem. Rev.* **122**, 16610–16751 (2022).

15. Xu, G.-L. *et al.* Challenges in Developing Electrodes, Electrolytes, and Diagnostics Tools to Understand and Advance Sodium-Ion Batteries. *Advanced Energy Materials* **8**, 1702403 (2018).

16. Nayak, P. K., Yang, L., Brehm, W. & Adelhelm, P. From lithium-ion to sodium-ion batteries: advantages, challenges, and surprises. *Angew. Chem., Int. Ed.* **57**, 102–120 (2018).

17. Rudola, A. *et al.* Commercialisation of high energy density sodium-ion batteries: Faradion's journey and outlook. *J. Mater. Chem. A* **9**, 8279–8302 (2021).

18. Zuo, W. *et al.* Nondestructive Analysis of Commercial Batteries. *Chem. Rev.* **125**, 369–444 (2025).

19. Hwang, J.-Y. *et al.* Radially aligned hierarchical columnar structure as a cathode material for high energy density sodium-ion batteries. *Nat Commun* **6**, 6865 (2015).

20. Zuo, W. *et al.* Microstrain screening towards defect-less layered transition metal

oxide cathodes. *Nat. Nanotechnol.* **19**, 1644–1653 (2024).

21. Xu, G.-L. *et al.* Native lattice strain induced structural earthquake in sodium layered oxide cathodes. *Nat Commun* **13**, 436 (2022).

22. Fang, C. *et al.* Routes to high energy cathodes of sodium-ion batteries. *Adv. Energy Mater.* **6**, 1501727 (2016).

23. Du, M. *et al.* Ultrafast Preparation of High-Entropy NASICON Cathode Enables Stabilized Multielectron Redox and Wide-Temperature (−50–60 °C) Workability in Sodium-Ion Batteries. *Advanced Materials* **n/a**, 2418219.

24. Kang, J. *et al.* High rate performance of a Na3V2(PO4)3/C cathode prepared by pyro-synthesis for sodium-ion batteries. *J. Mater. Chem.* **22**, 20857 (2012).

25. Zhou, W. *et al.* NaxMV(PO4)3 (M = Mn, Fe, Ni) Structure and Properties for Sodium Extraction. *Nano Lett.* **16**, 7836–7841 (2016).

26. Yabuuchi, N. *et al.* P2-type Nax[Fe1/2Mn1/2]O2 made from earth-abundant elements for rechargeable Na batteries. *Nat. Mater.* **11**, 512–517 (2012).

27. Wu, C. *et al.* Hard carbon for sodium-ion batteries: progress, strategies and future perspective. *Chem. Sci.* **15**, 6244–6268 (2024).

28. Dou, X. *et al.* Hard carbons for sodium-ion batteries: Structure, analysis, sustainability, and electrochemistry. *Materials Today* **23**, 87–104 (2019).

29. Hou, H., Qiu, X., Wei, W., Zhang, Y. & Ji, X. Carbon Anode Materials for Advanced Sodium-Ion Batteries. *Advanced Energy Materials* **7**, 1602898 (2017).

30. Zuo, W. *et al.* Layered Oxide Cathodes for Sodium-Ion Batteries: Storage

Mechanism, Electrochemistry, and Techno-economics. *Acc. Chem. Res.* **56**, 284–296 (2023).

31. Senguttuvan, P., Rousse, G., Seznec, V., Tarascon, J.-M. & Palacín, M. R. Na2Ti3O7: Lowest Voltage Ever Reported Oxide Insertion Electrode for Sodium Ion Batteries. *Chem. Mater.* **23**, 4109–4111 (2011).

32. Pan, H. *et al.* Sodium Storage and Transport Properties in Layered Na2Ti3O7 for Room-Temperature Sodium-Ion Batteries. *Advanced Energy Materials* **3**, 1186–1194 (2013).

33. Cao, Y. *et al.* A New Triclinic Phase Na2Ti3O7 Anode for Sodium-Ion Battery. *Advanced Functional Materials* **30**, 2003733 (2020).

34. Knehr, K. W., Kubal, J. J., Nelson, P. A. & Ahmed, S. *Battery Performance and Cost Modeling for Electric-Drive Vehicles (A Manual for BatPaC v5.0)*. https://www.osti.gov/biblio/1877590 (2022) doi:10.2172/1877590.

35. Yao, A., Benson, S. M. & Chueh, W. C. Critically assessing sodium-ion technology roadmaps and scenarios for techno-economic competitiveness against lithium-ion batteries. *Nat Energy* **10**, 404–416 (2025).

36. Mu, L. *et al.* Prototype Sodium-Ion Batteries Using an Air-Stable and Co/Ni-Free O3-Layered Metal Oxide Cathode. *Advanced Materials* **27**, 6928–6933 (2015).

37. Ding, F. *et al.* Tailoring Electronic Structure to Achieve Maximum Utilization of Transition Metal Redox for High-Entropy Na Layered Oxide Cathodes. *J. Am. Chem. Soc.* **145**, 13592–13602 (2023).

38. Zhao, C., Ding, F., Lu, Y., Chen, L. & Hu, Y.-S. High-Entropy Layered Oxide Cathodes for Sodium-Ion Batteries. *Angewandte Chemie International Edition* **59**, 264–269 (2020).

39. Xu, G.-L. *et al.* Insights into the structural effects of layered cathode materials for high voltage sodium-ion batteries. *Energy Environ. Sci.* **10**, 1677–1693 (2017).

40. Ding, F. *et al.* Tailoring planar strain for robust structural stability in high-entropy layered sodium oxide cathode materials. *Nat Energy* **9**, 1529–1539 (2024).

41. Zuo, W. *et al.* Engineering Na+-layer spacings to stabilize Mn-based layered cathodes for sodium-ion batteries. *Nature Communications* **12**, 4903 (2021).

42. Li, Y., Lu, Y., Adelhelm, P., Titirici, M.-M. & Hu, Y.-S. Intercalation chemistry of graphite: alkali metal ions and beyond. *Chem. Soc. Rev.* **48**, 4655–4687 (2019).

43. Novák, P. *et al.* The complex electrochemistry of graphite electrodes in lithium-ion batteries. *Journal of Power Sources* **97–98**, 39–46 (2001).

44. Ge, P. & Fouletier, M. Electrochemical intercalation of sodium in graphite. *Solid State Ionics* **28–30**, 1172–1175 (1988).

45. Stevens, D. A. & Dahn, J. R. High Capacity Anode Materials for Rechargeable Sodium-Ion Batteries. *J. Electrochem. Soc.* **147**, 1271 (2000).

46. Bommier, C., Surta, T. W., Dolgos, M. & Ji, X. New Mechanistic Insights on Na-Ion Storage in Nongraphitizable Carbon. *Nano Lett.* **15**, 5888–5892 (2015).

47. Li, Y. *et al.* Origin of fast charging in hard carbon anodes. *Nat Energy* **9**, 134–142 (2024).

48. Li, Z. *et al.* Defective Hard Carbon Anode for Na-Ion Batteries. *Chem. Mater.* **30**, 4536–4542 (2018).

49. Chen, C. *et al.* Multi-heteroatom doped porous carbon derived from insect feces for capacitance-enhanced sodium-ion storage. *Journal of Energy Chemistry* **54**, 482–492 (2021).

50. Mehmood, A. *et al.* Nanoporous nitrogen doped carbons with enhanced capacity for sodium ion battery anodes. *Energy Storage Materials* **28**, 101–111 (2020).

51. Qiu, S. *et al.* Manipulating Adsorption–Insertion Mechanisms in Nanostructured Carbon Materials for High-Efficiency Sodium Ion Storage. *Advanced Energy Materials* **7**, 1700403 (2017).

52. Li, Y., Hu, Y.-S., Titirici, M.-M., Chen, L. & Huang, X. Hard Carbon Microtubes Made from Renewable Cotton as High-Performance Anode Material for Sodium-Ion Batteries. *Advanced Energy Materials* **6**, 1600659 (2016).

53. Morikawa, Y., Nishimura, S., Hashimoto, R., Ohnuma, M. & Yamada, A. Mechanism of Sodium Storage in Hard Carbon: An X-Ray Scattering Analysis. *Advanced Energy Materials* **10**, 1903176 (2020).

54. Gotoh, K. *et al.* NMR study for electrochemically inserted Na in hard carbon electrode of sodium ion battery. *Journal of Power Sources* **225**, 137–140 (2013).

55. Liu, X. *et al.* Evidence of Quasi-Na Metallic Clusters in Sodium Ion Batteries through In Situ X-Ray Diffraction. *Advanced Materials* **37**, 2410673 (2025).

56. Au, H. *et al.* A revised mechanistic model for sodium insertion in hard carbons.

Energy & Environmental Science **13**, 3469–3479 (2020).

57. M. Stratford, J., K. Allan, P., Pecher, O., A. Chater, P. & P. Grey, C. Mechanistic insights into sodium storage in hard carbon anodes using local structure probes. *Chemical Communications* **52**, 12430–12433 (2016).

58. Zheng, Y. *et al.* Superior electrochemical performance of sodium-ion full-cell using poplar wood derived hard carbon anode. *Energy Storage Materials* **18**, 269–279 (2019).

59. Tang, Z. *et al.* Revealing the closed pore formation of waste wood-derived hard carbon for advanced sodium-ion battery. *Nat Commun* **14**, 6024 (2023).

60. Xu, T., Qiu, X., Zhang, X. & Xia, Y. Regulation of surface oxygen functional groups and pore structure of bamboo-derived hard carbon for enhanced sodium storage performance. *Chemical Engineering Journal* **452**, 139514 (2023).

61. Wang, Q. *et al.* Rice husk-derived hard carbons as high-performance anode materials for sodium-ion batteries. *Carbon* **127**, 658–666 (2018).

62. Liu, P. *et al.* A waste biomass derived hard carbon as a high-performance anode material for sodium-ion batteries. *Journal of Materials Chemistry A* **4**, 13046–13052 (2016).

63. Chen, C. *et al.* Nonignorable Influence of Oxygen in Hard Carbon for Sodium Ion Storage. *ACS Sustainable Chem. Eng.* **8**, 1497–1506 (2020).

64. Nita, C., Zhang, B., Dentzer, J. & Matei Ghimbeu, C. Hard carbon derived from coconut shells, walnut shells, and corn silk biomass waste exhibiting high capacity for Na-

ion batteries. *Journal of Energy Chemistry* **58**, 207–218 (2021).

65. Chen, B. *et al.* Lignin molecular sieving engineering enables high-plateau-capacity hard carbon anodes for sodium-ion batteries. *Green Chemistry* **26**, 7919–7930 (2024).

66. Huang, Z., Huang, J., Zhong, L., Zhang, W. & Qiu, X. Deconstruction Engineering of Lignocellulose Toward High-Plateau-Capacity Hard Carbon Anodes for Sodium-Ion Batteries. *Small* **20**, 2405632 (2024).

67. He, X.-X. *et al.* Achieving All-Plateau and High-Capacity Sodium Insertion in Topological Graphitized Carbon. *Advanced Materials* **35**, 2302613 (2023).

68. Wu, S. *et al.* Nitrogen/phosphorus co-doped ultramicropores hard carbon spheres for rapid sodium storage. *Carbon* **218**, 118756 (2024).

69. Asfaw, H. D., Tai, C.-W., Valvo, M. & Younesi, R. Facile synthesis of hard carbon microspheres from polyphenols for sodium-ion batteries: insight into local structure and interfacial kinetics. *Materials Today Energy* **18**, 100505 (2020).

70. Li, N. *et al.* Phosphorus-doped hard carbon with controlled active groups and microstructure for high-performance sodium-ion batteries. *Journal of Materials Chemistry A* **8**, 20486–20492 (2020).

71. Beda, A., Taberna, P.-L., Simon, P. & Matei Ghimbeu, C. Hard carbons derived from green phenolic resins for Na-ion batteries. *Carbon* **139**, 248–257 (2018).

72. Xu, Z. *et al.* The Role of Hydrothermal Carbonization in Sustainable Sodium-Ion Battery Anodes. *Advanced Energy Materials* **12**, 2200208 (2022).

73. Väli, R., Jänes, A., Thomberg, T. & Lust, E. D-Glucose Derived Nanospheric Hard Carbon Electrodes for Room-Temperature Sodium-Ion Batteries. *J. Electrochem. Soc.* **163**, A1619 (2016).

74. Oğuzhan Eren, E. *et al.* Hard carbon from a sugar derivative for next-generation sodium-ion batteries. *Materials Horizons* **12**, 886–898 (2025).

75. Zheng, Z. *et al.* CO2-Etching Creates Abundant Closed Pores in Hard Carbon for High-Plateau-Capacity Sodium Storage. *Advanced Energy Materials* **14**, 2303064 (2024).

76. Chen, H., Sun, N., Wang, Y., Soomro, R. A. & Xu, B. One stone two birds: Pitch assisted microcrystalline regulation and defect engineering in coal-based carbon anodes for sodium-ion batteries. *Energy Storage Materials* **56**, 532–541 (2023).

77. Liu, X. *et al.* Potato-starch-based hard carbon microspheres: Preparation and application as an anode material for sodium-ion batteries. *Solid State Ionics* **406**, 116475 (2024).

78. Gomez-Martin, A. *et al.* Correlation of Structure and Performance of Hard Carbons as Anodes for Sodium Ion Batteries. *Chem. Mater.* **31**, 7288–7299 (2019).

79. Xiao, L. *et al.* Low-Defect and Low-Porosity Hard Carbon with High Coulombic Efficiency and High Capacity for Practical Sodium Ion Battery Anode. *Advanced Energy Materials* **8**, 1703238 (2018).

80. Buiel, E. R., George, A. E. & Dahn, J. R. Model of micropore closure in hard carbon prepared from sucrose. *Carbon* **37**, 1399–1407 (1999).

81. Zhang, X. *et al.* Exploring Carbonization Temperature to Create Closed Pores for

Hard Carbon as High-Performance Sodium-Ion Battery Anodes. *Small* **20**, 2311197 (2024).

82. Lakienko, G. P. *et al.* Design of the Particle Size and Morphology of Hard Carbon Anode Materials for Sodium-Ion Batteries Through Hydrothermal Carbonization. *J. Electrochem. Soc.* **171**, 060512 (2024).

83. Nagmani, Manna, S. & Puravankara, S. Hierarchically porous closed-pore hard carbon as a plateau-dominated high-performance anode for sodium-ion batteries. *Chemical Communications* **60**, 3071–3074 (2024).

84. Yu, K., Wang, X., Yang, H., Bai, Y. & Wu, C. Insight to defects regulation on sugarcane waste-derived hard carbon anode for sodium-ion batteries. *Journal of Energy Chemistry* **55**, 499–508 (2021).

85. Hong, K. *et al.* Biomass derived hard carbon used as a high performance anode material for sodium ion batteries. *Journal of Materials Chemistry A* **2**, 12733–12738 (2014).

86. Matei Ghimbeu, C., Zhang, B., Martinez de Yuso, A., Réty, B. & Tarascon, J.-M. Valorizing low cost and renewable lignin as hard carbon for Na-ion batteries: Impact of lignin grade. *Carbon* **153**, 634–647 (2019).

87. Liu, J. *et al.* Precisely Tunable Instantaneous Carbon Rearrangement Enables Low-Working-Potential Hard Carbon Toward Sodium-Ion Batteries with Enhanced Energy Density. *Advanced Materials* **36**, 2407369 (2024).

88. Zhen, Y. *et al.* Ultrafast synthesis of hard carbon anodes for sodium-ion batteries. *Proceedings of the National Academy of Sciences* **118**, e2111119118 (2021).

89. Ryoo, G. *et al.* Ultrafast Synthesis of Hard Carbon Anodes for Sodium-ion

Batteries: An Intense-Pulsed-Light-Assisted Approach to Photothermal Carbonization of Polymer/Carbon Nanotube Composite Films. *Small Methods* **n/a**, 2401801.

90. Ryoo, G. *et al.* Sub-minute carbonization of polymer/carbon nanotube films by microwave induction heating for ultrafast preparation of hard carbon anodes for sodium-ion batteries. *Chemical Engineering Journal* **496**, 154081 (2024).

91. Yan, J. *et al.* Ultrahigh Phosphorus Doping of Carbon for High-Rate Sodium Ion Batteries Anode. *Advanced Energy Materials* **11**, 2003911 (2021).

92. Sun, F. *et al.* Carboxyl-Dominant Oxygen Rich Carbon for Improved Sodium Ion Storage: Synergistic Enhancement of Adsorption and Intercalation Mechanisms. *Advanced Energy Materials* **11**, 2002981 (2021).

93. Li, Y. *et al.* Insights into the Na+ Storage Mechanism of Phosphorus-Functionalized Hard Carbon as Ultrahigh Capacity Anodes. *Advanced Energy Materials* **8**, 1702781 (2018).

94. Li, Z. *et al.* Mechanism of Na-Ion Storage in Hard Carbon Anodes Revealed by Heteroatom Doping. *Advanced Energy Materials* **7**, 1602894 (2017).

95. Qi, Y. *et al.* Slope-Dominated Carbon Anode with High Specific Capacity and Superior Rate Capability for High Safety Na-Ion Batteries. *Angewandte Chemie International Edition* **58**, 4361–4365 (2019).

96. Xie, F. *et al.* Screening Heteroatom Configurations for Reversible Sloping Capacity Promises High-Power Na-Ion Batteries. *Angewandte Chemie International Edition* **61**, e202116394 (2022).

97. Tang, X. *et al.* Kinetics Manipulation for Improved Solid Electrolyte Interphase and Reversible Na Storage. *ACS Energy Lett.* **9**, 1158–1167 (2024).

98. Manna, S. & Puravankara, S. Revealing the storage mechanism of plateau-dominated S-doped hard carbon as high-performance anode for sodium-ion batteries. *Next Materials* **7**, 100353 (2025).

99. Wu, F. *et al.* Expanding Interlayer Spacing of Hard Carbon by Natural K+ Doping to Boost Na-Ion Storage. *ACS Appl. Mater. Interfaces* **10**, 27030–27038 (2018).

100. Li, Y. *et al.* Dual-Functionalized Ca Enables High Sodiation Kinetics for Hard Carbon in Sodium-Ion Batteries. *ACS Appl. Mater. Interfaces* **16**, 2397–2407 (2024).

101. Li, Y. *et al.* Regulating Pore Structure of Hierarchical Porous Waste Cork-Derived Hard Carbon Anode for Enhanced Na Storage Performance. *Advanced Energy Materials* **9**, 1902852 (2019).

102. Song, M. *et al.* Towards enhanced sodium storage of hard carbon anodes: Regulating the oxygen content in precursor by low-temperature hydrogen reduction. *Energy Storage Materials* **51**, 620–629 (2022).

103. Lin, X., Liu, Y., Tan, H. & Zhang, B. Advanced lignin-derived hard carbon for Na-ion batteries and a comparison with Li and K ion storage. *Carbon* **157**, 316–323 (2020).

104. Hou, B.-H. *et al.* Self-Supporting, Flexible, Additive-Free, and Scalable Hard Carbon Paper Self-Interwoven by 1D Microbelts: Superb Room/Low-Temperature Sodium Storage and Working Mechanism. *Advanced Materials* **31**, 1903125 (2019).

105. Wei, Z. *et al.* Insights into the pre-oxidation process of phenolic resin-based hard carbon for sodium storage. *Mater. Chem. Front.* **5**, 3911–3917 (2021).

106. Shen, C. *et al.* Tailoring the Surface Chemistry of Hard Carbon Towards High-Efficiency Sodium Ion Storage. *Nanoscale* **14**, (2022).

107. Meng, Q. *et al.* Tuning the Closed Pore Structure of Hard Carbons with the Highest Na Storage Capacity. *ACS Energy Lett.* **4**, 2608–2612 (2019).

108. Guo, M. *et al.* Liquid Template Assisted Activation for "Egg Puff"-Like Hard Carbon toward High Sodium Storage Performance. *Small* **19**, 2302583 (2023).

109. Kamiyama, A. *et al.* MgO-Template Synthesis of Extremely High Capacity Hard Carbon for Na-Ion Battery. *Angewandte Chemie International Edition* **60**, 5114–5120 (2021).

110. Wang, K. *et al.* Altering Thermal Transformation Pathway to Create Closed Pores in Coal-Derived Hard Carbon and Boosting of Na+ Plateau Storage for High-Performance Sodium-Ion Battery and Sodium-Ion Capacitor. *Advanced Functional Materials* **32**, 2203725 (2022).

111. Lu, Z. *et al.* Zinc Single-Atom-Regulated Hard Carbons for High-Rate and Low-Temperature Sodium-Ion Batteries. *Advanced Materials* **35**, 2211461 (2023).

112. Yuan, M. *et al.* A General Multi-Interface Strategy toward Densified Carbon Materials with Enhanced Comprehensive Electrochemical Performance for Li/Na-Ion Batteries. *Small* **18**, 2105738 (2022).

113. Huang, Y. *et al.* Rationally Designing Closed Pore Structure by Carbon Dots

to Evoke Sodium Storage Sites of Hard Carbon in Low-Potential Region. *Advanced Functional Materials* **34**, 2308392 (2024).

114. Cheng, M.-G. *et al.* Preparation of Enriched Closed-Pores Hard Carbon for High-Performance Sodium-Ion Batteries by the Poly(vinyl butyral) Template Method. *ACS Appl. Energy Mater.* **7**, 3452–3461 (2024).

115. Yin, X. *et al.* Enabling Fast Na+ Transfer Kinetics in the Whole-Voltage-Region of Hard-Carbon Anodes for Ultrahigh-Rate Sodium Storage. *Advanced Materials* **34**, 2109282 (2022).

116. Huang, S. *et al.* N-Doping and Defective Nanographitic Domain Coupled Hard Carbon Nanoshells for High Performance Lithium/Sodium Storage. *Advanced Functional Materials* **28**, 1706294 (2018).

117. Yu, Z.-L. *et al.* Ion-Catalyzed Synthesis of Microporous Hard Carbon Embedded with Expanded Nanographite for Enhanced Lithium/Sodium Storage. *J. Am. Chem. Soc.* **138**, 14915–14922 (2016).

118. Jin, Q. *et al.* Designing a slope-dominated hybrid nanostructure hard carbon anode for high-safety and high-capacity Na-ion batteries. *J. Mater. Chem. A* **8**, 22613–22619 (2020).

119. Zhao, J. *et al.* Catalytic Defect-Repairing Using Manganese Ions for Hard Carbon Anode with High-Capacity and High-Initial-Coulombic-Efficiency in Sodium-Ion Batteries. *Advanced Energy Materials* **13**, 2300444 (2023).

120. Li, Q. *et al.* Sieving carbons promise practical anodes with extensible low-

potential plateaus for sodium batteries. *National Science Review* **9**, nwac084 (2022).

121. Deng, W. *et al.* Catalyst-Assisted Chemical Vapor Deposition Engineering of Hard Carbon with Abundant Closed Pores for High-Performance Sodium-Ion Batteries. *Advanced Functional Materials* **n/a**, 2501721 (2025).

122. Fei, M. *et al.* Preformation of Insoluble Solid-Electrolyte Interphase for Highly Reversible Na-Ion Batteries. *Angewandte Chemie International Edition* **63**, e202409719 (2024).

123. Liu, M. *et al.* Interfacial-Catalysis-Enabled Layered and Inorganic-Rich SEI on Hard Carbon Anodes in Ester Electrolytes for Sodium-Ion Batteries. *Advanced Materials* **35**, 2300002 (2023).

124. Lu, H. *et al.* Engineering Al2O3 atomic layer deposition: Enhanced hard carbon-electrolyte interface towards practical sodium ion batteries. *Nano Energy* **64**, 103903 (2019).

125. Lu, Z. *et al.* Step-by-step desolvation enables high-rate and ultra-stable sodium storage in hard carbon anodes. *Proceedings of the National Academy of Sciences* **119**, e2210203119 (2022).

126. Zhao, X. *et al.* Unlocking plateau capacity with versatile precursor crosslinking for carbon anodes in Na-ion batteries. *Energy Storage Materials* **70**, 103543 (2024).

127. Xiao, S. *et al.* Insight into the Role of Closed-Pore Size on Rate Capability of Hard Carbon for Fast-Charging Sodium-Ion Batteries. *Advanced Materials* **37**, 2501434

(2025).

128. Zhao, C. *et al.* High-temperature treatment induced carbon anode with ultrahigh Na storage capacity at low-voltage plateau. *Science Bulletin* **63**, 1125–1129 (2018).

129. Müller, C. *et al.* Influences on Reliable Capacity Measurements of Hard Carbon in Highly Loaded Electrodes. *Batteries & Supercaps* **6**, e202300322 (2023).

130. Ji, W., Qu, H., Zhang, X., Zheng, D. & Qu, D. Electrode Architecture Design to Promote Charge-Transport Kinetics in High-Loading and High-Energy Lithium-Based Batteries. *Small Methods* **5**, 2100518 (2021).

131. Park, K.-Y. *et al.* Understanding capacity fading mechanism of thick electrodes for lithium-ion rechargeable batteries. *Journal of Power Sources* **468**, 228369 (2020).

132. Zhao, H., Yuan, W. & Liu, G. Hierarchical electrode design of high-capacity alloy nanomaterials for lithium-ion batteries. *Nano Today* **10**, 193–212 (2015).

133. Park, S.-H. *et al.* High areal capacity battery electrodes enabled by segregated nanotube networks. *Nat Energy* **4**, 560–567 (2019).

134. He, Y., Bai, P., Gao, S. & Xu, Y. Marriage of an Ether-Based Electrolyte with Hard Carbon Anodes Creates Superior Sodium-Ion Batteries with High Mass Loading. *ACS Appl. Mater. Interfaces* **10**, 41380–41388 (2018).

135. Hu, L. *et al.* Lithium-Ion Textile Batteries with Large Areal Mass Loading. *Advanced Energy Materials* **1**, 1012–1017 (2011).

136. Gallagher, K. G. *et al.* Optimizing Areal Capacities through Understanding the Limitations of Lithium-Ion Electrodes. *J. Electrochem. Soc.* **163**, A138 (2015).

137. Kim, J.-H. *et al.* Upscaling high-areal-capacity battery electrodes. *Nat Energy* **10**, 295–307 (2025).

138. Sun, C. *et al.* 3D printing nanocomposite gel-based thick electrode enabling both high areal capacity and rate performance for lithium-ion battery. *Chemical Engineering Journal* **381**, 122641 (2020).

139. Ryu, M., Hong, Y.-K., Lee, S.-Y. & Park, J. H. Ultrahigh loading dry-process for solvent-free lithium-ion battery electrode fabrication. *Nat Commun* **14**, 1316 (2023).

140. Zhang, W. *et al.* Enhanced interphasial stability of hard carbon for sodium-ion battery via film-forming electrolyte additive. *Nano Res.* **16**, 3823–3831 (2023).

141. Wu, H. & Cui, Y. Designing nanostructured Si anodes for high energy lithium ion batteries. *Nano Today* **7**, 414–429 (2012).

142. Komaba, S. *et al.* Redox reaction of Sn-polyacrylate electrodes in aprotic Na cell. *Electrochemistry Communications* **21**, 65–68 (2012).

143. Ellis, L. D., Wilkes, B. N., Hatchard, T. D. & Obrovac, M. N. In Situ XRD Study of Silicon, Lead and Bismuth Negative Electrodes in Nonaqueous Sodium Cells. *J. Electrochem. Soc.* **161**, A416 (2014).

144. Jung, S. C., Jung, D. S., Choi, J. W. & Han, Y.-K. Atom-Level Understanding of the Sodiation Process in Silicon Anode Material. *J. Phys. Chem. Lett.* **5**, 1283–1288 (2014).

145. Jangid, M. K., Vemulapally, A., Sonia, F. J., Aslam, M. & Mukhopadhyay, A. Feasibility of Reversible Electrochemical Na-Storage and Cyclic Stability of Amorphous Silicon and Silicon-Graphene Film Electrodes. *J. Electrochem. Soc.* **164**, A2559 (2017).

146. Lim, C.-H. *et al.* Experimental Study on Sodiation of Amorphous Silicon for Use as Sodium-Ion Battery Anode. *Electrochimica Acta* **211**, 265–272 (2016).

147. Xu, Y. *et al.* Reversible Na-Ion Uptake in Si Nanoparticles. *Advanced Energy Materials* **6**, 1501436 (2016).

148. Shimizu, M., Usui, H., Fujiwara, K., Yamane, K. & Sakaguchi, H. Electrochemical behavior of SiO as an anode material for Na-ion battery. *Journal of Alloys and Compounds* **640**, 440–443 (2015).

149. Loaiza, L. C., Monconduit, L. & Seznec, V. Si and Ge-Based Anode Materials for Li-, Na-, and K-Ion Batteries: A Perspective from Structure to Electrochemical Mechanism. *Small* **16**, 1905260 (2020).

150. Xu, G.-L. *et al.* Nanostructured Black Phosphorus/Ketjenblack–Multiwalled Carbon Nanotubes Composite as High Performance Anode Material for Sodium-Ion Batteries. *Nano Lett.* **16**, 3955–3965 (2016).

151. Sui, Y. *et al.* Recent advances in black-phosphorus-based materials for electrochemical energy storage. *Materials Today* **42**, 117–136 (2021).

152. Lin, S., Li, Y., Qian, J. & Lau, S. P. Emerging opportunities for black phosphorus in energy applications. *Materials Today Energy* **12**, 1–25 (2019).

153. Yang, F., Gao, H., Chen, J. & Guo, Z. Phosphorus-Based Materials as the

Anode for Sodium-Ion Batteries. *Small Methods* **1**, 1700216 (2017).

154. Baggetto, L., Keum, J. K., Browning, J. F. & Veith, G. M. Germanium as negative electrode material for sodium-ion batteries. *Electrochemistry Communications* **34**, 41–44 (2013).

155. Jung, S. C., Kim, H.-J., Kang, Y.-J. & Han, Y.-K. Advantages of Ge anode for Na-ion batteries: Ge vs. Si and Sn. *Journal of Alloys and Compounds* **688**, 158–163 (2016).

156. Ahad, S. A. *et al.* Amorphization driven Na-alloying in SixGe1−x alloy nanowires for Na-ion batteries. *J. Mater. Chem. A* **9**, 20626–20634 (2021).

157. Datta, M. K. *et al.* Tin and graphite based nanocomposites: Potential anode for sodium ion batteries. *Journal of Power Sources* **225**, 316–322 (2013).

158. Ellis, L. D., Hatchard, T. D. & Obrovac, M. N. Reversible Insertion of Sodium in Tin. *J. Electrochem. Soc.* **159**, A1801 (2012).

159. Li, Z., Ding, J. & Mitlin, D. Tin and Tin Compounds for Sodium Ion Battery Anodes: Phase Transformations and Performance. *Acc. Chem. Res.* **48**, 1657–1665 (2015).

160. Wu, X. *et al.* Tin-Based Anode Materials for Stable Sodium Storage: Progress and Perspective. *Advanced Materials* **34**, 2106895 (2022).

161. Ding, X. *et al.* Tremendously excess Na-storage capacity of Sb@C anode towards high-performance sodium-ion batteries. *Chemical Engineering Journal* **505**, 159402 (2025).

162. Sarkar, S. & Peter, S. C. An overview on Sb-based intermetallics and alloys for sodium-ion batteries: trends, challenges and future prospects from material synthesis to

battery performance. *J. Mater. Chem. A* **9**, 5164–5196 (2021).

163. Mun, Y. S. *et al.* Copper–antimony–red phosphorus composites as promising anode materials for sodium-ion batteries. *Journal of Power Sources* **362**, 115–122 (2017).

164. Jow, T. R., Shacklette, L. W., Maxfield, M. & Vernick, D. The Role of Conductive Polymers in Alkali-Metal Secondary Electrodes. *J. Electrochem. Soc.* **134**, 1730 (1987).

165. Garayt, M. D. L. *et al.* Restructuring of Sodium-Lead Alloys during Charge-Discharge Cycling in Sodium-Ion Batteries. *J. Electrochem. Soc.* **171**, 120521 (2024).

166. Eaves-Rathert, J., Moyer-Vanderburgh, K., Wolfe, K., Zohair, M. & Pint, C. L. Leveraging impurities in recycled lead anodes for sodium-ion batteries. *Energy Storage Materials* **53**, 552–558 (2022).

167. Xiong, P. *et al.* Bismuth Nanoparticle@Carbon Composite Anodes for Ultralong Cycle Life and High-Rate Sodium-Ion Batteries. *Advanced Materials* **31**, 1904771 (2019).

168. Wang, C., Wang, L., Li, F., Cheng, F. & Chen, J. Bulk Bismuth as a High-Capacity and Ultralong Cycle-Life Anode for Sodium-Ion Batteries by Coupling with Glyme-Based Electrolytes. *Advanced Materials* **29**, 1702212 (2017).

169. Zuo, W., Xu, P., Li, Y. & Liu, J. Direct growth of bismuth film as anode for aqueous rechargeable batteries in LiOH, NaOH and KOH electrolytes. *Nanomaterials* **5**, 1756–1765 (2015).

170. Zhao, Y., R. Adair, K. & Sun, X. Recent developments and insights into the

understanding of Na metal anodes for Na-metal batteries. *Energy & Environmental Science* **11**, 2673–2695 (2018).

171. Deng, T. *et al.* Interfacial-engineering-enabled practical low-temperature sodium metal battery. *Nat. Nanotechnol.* **17**, 269–277 (2022).

172. Home | ICSD. https://icsd.products.fiz-karlsruhe.de/en.

173. Materials Project. *Materials Project* https://next-gen.materialsproject.org/.

174. Kim, D., Zhang, K., Cho, M. & Kang, Y.-M. Critical design factors for kinetically favorable P-based compounds toward alloying with Na ions for high-power sodium-ion batteries. *Energy & Environmental Science* **12**, 1326–1333 (2019).

175. Liu, Y. *et al.* Red-phosphorus-impregnated carbon nanofibers for sodium-ion batteries and liquefaction of red phosphorus. *Nature communications* **11**, 2520 (2020).

176. Walter, M., Erni, R. & Kovalenko, M. V. Inexpensive antimony nanocrystals and their composites with red phosphorus as high-performance anode materials for Na-ion batteries. *Scientific reports* **5**, 8418 (2015).

177. Xie, H. *et al.* Sn–Bi–Sb alloys as anode materials for sodium ion batteries. *J. Mater. Chem. A* **5**, 9661–9670 (2017).

178. Wang, J. W., Liu, X. H., Mao, S. X. & Huang, J. Y. Microstructural Evolution of Tin Nanoparticles during In Situ Sodium Insertion and Extraction. *Nano Lett.* **12**, 5897–5902 (2012).

179. Palaniselvam, T. *et al.* Sodium Storage and Electrode Dynamics of Tin–Carbon Composite Electrodes from Bulk Precursors for Sodium-Ion Batteries. *Advanced*

Functional Materials **29**, 1900790 (2019).

180. Abundance of elements in Earth's crust. *Wikipedia* (2025).

181. Peng, M. *et al.* Alloy-Type Anodes for High-Performance Rechargeable Batteries. *Angewandte Chemie* **134**, e202206770 (2022).

182. Ramireddy, T. *et al.* Phosphorus–carbon nanocomposite anodes for lithium-ion and sodium-ion batteries. *Journal of Materials Chemistry A* **3**, 5572–5584 (2015).

183. Zhou, J. *et al.* Wet-Chemical Synthesis of Hollow Red-Phosphorus Nanospheres with Porous Shells as Anodes for High-Performance Lithium-Ion and Sodium-Ion Batteries. *Advanced Materials* **29**, 1700214 (2017).

184. Zhang, Y. *et al.* Red phosphorus confined in N-doped multi-cavity mesoporous carbon for ultrahigh-performance sodium-ion batteries. *Journal of Power Sources* **450**, 227696 (2020).

185. Liu, W. *et al.* Encapsulation of Red Phosphorus in Carbon Nanocages with Ultrahigh Content for High-Capacity and Long Cycle Life Sodium-Ion Batteries. *ACS Nano* **15**, 5679–5688 (2021).

186. Ma, X., Ji, C., Li, X., Liu, Y. & Xiong, X. Red@ Black phosphorus core–shell heterostructure with superior air stability for high-rate and durable sodium-ion battery. *Materials Today* **59**, 36–45 (2022).

187. Liu, X. *et al.* Stress- and Interface-Compatible Red Phosphorus Anode for High-Energy and Durable Sodium-Ion Batteries. *ACS Energy Lett.* **6**, 547–556 (2021).

188. Daali, A., Amine, R., Otieno, W., Xu, G.-L. & Amine, K. Strategies to enable

microsized alloy anodes for high-energy and long-life alkali-ion batteries. *Industrial Chemistry & Materials* **2**, 489–513 (2024).

189. Tian, Y., An, Y. & Zhang, B. Approaching Microsized Alloy Anodes via Solid Electrolyte Interphase Design for Advanced Rechargeable Batteries. *Advanced Energy Materials* **13**, 2300123 (2023).

190. Tian, H., Tan, X., Xin, F., Wang, C. & Han, W. Micro-sized nano-porous Si/C anodes for lithium ion batteries. *Nano Energy* **11**, 490–499 (2015).

191. Cong, L., Xie, H. & Li, J. Hierarchical Structures Based on Two-Dimensional Nanomaterials for Rechargeable Lithium Batteries. *Advanced Energy Materials* **7**, 1601906 (2017).

192. Guo, S. *et al.* Multiscale Micro-Nano Hierarchical Porous Germanium with Self-Adaptive Stress Dispersion for Highly Robust Lithium-Ion Batteries Anode. *Advanced Energy Materials* **14**, 2303876 (2024).

193. Li, S. *et al.* Yolk–Shell Sn@C Eggette-like Nanostructure: Application in Lithium-Ion and Sodium-Ion Batteries. *ACS Appl. Mater. Interfaces* **8**, 19438–19445 (2016).

194. Wu, L. *et al.* A Sn–SnS–C nanocomposite as anode host materials for Na-ion batteries. *J. Mater. Chem. A* **1**, 7181–7184 (2013).

195. Xu, H., Liu, D., Wang, W. & Yu, G. Selenium-Doped Amorphous Black Phosphorus@TiO_2 /C Heterostructures for High-Performance Li/Na/K Ion Batteries. *Inorg. Chem.* **61**, 3121–3131 (2022).

196. Kim, S.-O. & Manthiram, A. High-Performance Red P-Based P–TiP_2 –C Nanocomposite Anode for Lithium-Ion and Sodium-Ion Storage. *Chem. Mater.* **28**, 5935–5942 (2016).

197. Wang, Z. *et al.* Constructing N-Doped porous carbon confined FeSb alloy nanocomposite with Fe-N-C coordination as a universal anode for advanced Na/K-ion batteries. *Chemical Engineering Journal* **384**, 123327 (2020).

198. Kim, I. T., Allcorn, E. & Manthiram, A. High-Performance MSb–Al2O3–C (M=Fe, Ni, and Cu) Nanocomposite-Alloy Anodes for Sodium-Ion Batteries. *Energy Technology* **1**, 319–326 (2013).

199. Chen, J. *et al.* Electrolyte design for LiF-rich solid–electrolyte interfaces to enable high-performance microsized alloy anodes for batteries. *Nat Energy* **5**, 386–397 (2020).

200. Zhou, L. *et al.* Electrolyte Engineering Enables High Stability and Capacity Alloying Anodes for Sodium and Potassium Ion Batteries. *ACS Energy Lett.* **5**, 766–776 (2020).

201. Zeng, Z. *et al.* Safer lithium ion batteries based on nonflammable electrolyte. *Journal of Power Sources* **279**, 6–12 (2015).

202. Ma, L. A., Naylor, A. J., Nyholm, L. & Younesi, R. Strategies for Mitigating Dissolution of Solid Electrolyte Interphases in Sodium-Ion Batteries. *Angewandte Chemie International Edition* **60**, 4855–4863 (2021).

203. Wang, S., Shi, J., Liu, Z. & Xia, Y. Advanced Ether-Based Electrolytes for

Lithium-ion Batteries. *Advanced Energy Materials* **14**, 2401526 (2024).

204. Zhao, H. *et al.* Effect of crown ether additive on the compatibility of electrolyte and hard carbon anode in sodium ion battery. *Journal of Alloys and Compounds* **948**, 169823 (2023).

205. Du, X. *et al.* Stabilizing Microsized Sn Anodes for Na-Ion Batteries with Extended Ether Electrolyte Chemistry. *ACS Appl. Energy Mater.* **5**, 2252–2259 (2022).

206. Xu, K. & Angell, C. A. Sulfone-Based Electrolytes for Lithium-Ion Batteries. *J. Electrochem. Soc.* **149**, A920 (2002).

207. Abouimrane, A., Belharouak, I. & Amine, K. Sulfone-based electrolytes for high-voltage Li-ion batteries. *Electrochemistry Communications* **11**, 1073–1076 (2009).

208. Jia, H. *et al.* Sulfone-based electrolytes for high energy density lithium-ion batteries. *Journal of Power Sources* **527**, 231171 (2022).

209. Jang, J. Y. *et al.* Interfacial architectures based on a binary additive combination for high-performance Sn4P3 anodes in sodium-ion batteries. *J. Mater. Chem. A* **3**, 8332–8338 (2015).

210. Ren, X. *et al.* Localized High-Concentration Sulfone Electrolytes for High-Efficiency Lithium-Metal Batteries. *Chem* **4**, 1877–1892 (2018).

211. Wu, M. *et al.* Toward an Ideal Polymer Binder Design for High-Capacity Battery Anodes. *J. Am. Chem. Soc.* **135**, 12048–12056 (2013).

212. He, Q. *et al.* Achievements, challenges, and perspectives in the design of polymer binders for advanced lithium-ion batteries. *Chemical Society Reviews* **53**, 7091–

7157 (2024).

213. Shi, Y., Zhou, X. & Yu, G. Material and Structural Design of Novel Binder Systems for High-Energy, High-Power Lithium-Ion Batteries. *Acc. Chem. Res.* **50**, 2642–2652 (2017).

214. Lee, S., Koo, H., Kang, H. S., Oh, K.-H. & Nam, K. W. Advances in Polymer Binder Materials for Lithium-Ion Battery Electrodes and Separators. *Polymers* **15**, 4477 (2023).

215. Zhao, H. *et al.* Conductive Polymer Binder for High-Tap-Density Nanosilicon Material for Lithium-Ion Battery Negative Electrode Application. *Nano Lett.* **15**, 7927–7932 (2015).

216. Wu, J. *et al.* Synergy of binders and electrolytes in enabling microsized alloy anodes for high performance potassium-ion batteries. *Nano Energy* **77**, 105118 (2020).

217. Yao, Q. *et al.* Intermolecular Cross-Linking Reinforces Polymer Binders for Durable Alloy-Type Anode Materials of Sodium-Ion Batteries. *Advanced Energy Materials* **13**, 2202939 (2023).

218. Bai, M. *et al.* An in-situ polymerization strategy for gel polymer electrolyte Si||Ni-rich lithium-ion batteries. *Nat Commun* **15**, 5375 (2024).

219. Huang, Q. *et al.* Supremely elastic gel polymer electrolyte enables a reliable electrode structure for silicon-based anodes. *Nat Commun* **10**, 5586 (2019).

220. Tolganbek, N. *et al.* Design and preparation of thin film gel polymer electrolyte for 3D Li-ion battery. *Journal of Power Sources* **493**, 229686 (2021).

221. Zhou, X. *et al.* Gel polymer electrolytes for rechargeable batteries toward wide-temperature applications. *Chemical Society Reviews* **53**, 5291–5337 (2024).

222. Aruchamy, K. *et al.* Gel Polymer Electrolytes: Advancing Solid-State Batteries for High-Performance Applications. *Gels* **9**, 585 (2023).

223. Zheng, J. *et al.* Progress in Gel Polymer Electrolytes for Sodium-Ion Batteries. *ENERGY & ENVIRONMENTAL MATERIALS* **6**, e12422 (2023).

224. Lee, J. H., Kim, S., Cho, M., Chanthad, C. & Lee, Y. Crosslinked Gel Polymer Electrolytes for Si Anodes in Li-Ion Batteries. *J. Electrochem. Soc.* **166**, A2755 (2019).

225. Hoang Huy, V. P., So, S. & Hur, J. Inorganic Fillers in Composite Gel Polymer Electrolytes for High-Performance Lithium and Non-Lithium Polymer Batteries. *Nanomaterials* **11**, 614 (2021).

226. Gel Polymer Electrolytes for Electrochemical Energy Storage - Cheng - 2018 - Advanced Energy Materials - Wiley Online Library. https://advanced.onlinelibrary.wiley.com/doi/full/10.1002/aenm.201702184.

227. Kim, Y. *et al.* An Amorphous Red Phosphorus/Carbon Composite as a Promising Anode Material for Sodium Ion Batteries. *Advanced Materials* **25**, 3045–3049 (2013).

228. Sun, J. *et al.* A phosphorene–graphene hybrid material as a high-capacity anode for sodium-ion batteries. *Nature nanotechnology* **10**, 980–985 (2015).

229. Ren, X. *et al.* Sn-C bonding riveted SnSe nanoplates vertically grown on nitrogen-doped carbon nanobelts for high-performance sodium-ion battery anodes. *Nano*

Energy **54**, 322–330 (2018).

230. Jung, S. C., Choi, J.-H. & Han, Y.-K. The origin of excellent rate and cycle performance of Sn4P3 binary electrodes for sodium-ion batteries. *J. Mater. Chem. A* **6**, 1772–1779 (2018).

231. Wang, W., Zhang, J., Yu, D. Y. W. & Li, Q. Improving the cycling stability of Sn4P3 anode for sodium-ion battery. *Journal of Power Sources* **364**, 420–425 (2017).

232. Kravets, Y., Sun, Y., Wang, H. & Adelhelm, P. Role of Silicon as Structural Stabilizer and Redox-Active Element in Multicomponent (Sn, Sb, Fe, Si) Alloy Electrodes for Na-Ion Batteries. *Batteries & Supercaps* **8**, e202400690 (2025).

233. Wu, C., Zhu, G., Wang, Q., Wu, M. & Zhang, H. Sn-based nanomaterials: From composition and structural design to their electrochemical performances for Li- and Na-ion batteries. *Energy Storage Materials* **43**, 430–462 (2021).

234. Lan, D. *et al.* Phase pure Sn4P3 nanotops by solution-liquid-solid growth for anode application in sodium ion batteries. *J. Mater. Chem. A* **5**, 5791–5796 (2017).

235. Fan, W., Gao, Y., Liu, H. & Xia, X. Rational design of conductive MXenes-based networks by Sn and Sn4P3 nanoparticles for durable sodium-ion battery. *Journal of Power Sources* **562**, 232750 (2023).

236. Sha, M. *et al.* Sn nanoparticles@nitrogen-doped carbon nanofiber composites as high-performance anodes for sodium-ion batteries. *J. Mater. Chem. A* **5**, 6277–6283 (2017).

237. Liu, N. *et al.* A pomegranate-inspired nanoscale design for large-volume-

change lithium battery anodes. *Nature Nanotech* **9**, 187–192 (2014).

238. Daali, A. *et al.* Tuning working potential of silicon-phosphorus anode via microstructure control for high-energy lithium-ion batteries. *J Solid State Electrochem* **26**, 1919–1927 (2022).

239. Wu, F. *et al.* High-Mass-Loading Electrodes for Advanced Secondary Batteries and Supercapacitors. *Electrochem. Energ. Rev.* **4**, 382–446 (2021).

240. Chen, Y., Zhao, B., Yang, Y. & Cao, A. Toward High-Areal-Capacity Electrodes for Lithium and Sodium Ion Batteries. *Advanced Energy Materials* **12**, 2201834 (2022).

241. Kuang, Y., Chen, C., Kirsch, D. & Hu, L. Thick Electrode Batteries: Principles, Opportunities, and Challenges. *Advanced Energy Materials* **9**, 1901457 (2019).

242. Tao, R., Gu, Y., Du, Z., Lyu, X. & Li, J. Advanced electrode processing for lithium-ion battery manufacturing. *Nat. Rev. Clean Technol.* **1**, 116–131 (2025).

243. Zheng, J. *et al.* Strategies and Challenge of Thick Electrodes for Energy Storage: A Review. *Batteries* **9**, 151 (2023).

244. Du, Z., Wood, D. L., Daniel, C., Kalnaus, S. & Li, J. Understanding limiting factors in thick electrode performance as applied to high energy density Li-ion batteries. *J Appl Electrochem* **47**, 405–415 (2017).

245. Evanoff, K. *et al.* Towards Ultrathick Battery Electrodes: Aligned Carbon Nanotube – Enabled Architecture. *Advanced Materials* **24**, 533–537 (2012).

246. Xie, F., Lu, Y., Chen, L. & Hu, Y.-S. Recent Progress in Presodiation

Technique for High-Performance Na-Ion Batteries. *Chinese Phys. Lett.* **38**, 118401 (2021).

247. Hu, Y.-S. & Li, Y. Unlocking Sustainable Na-Ion Batteries into Industry. *ACS Energy Lett.* **6**, 4115–4117 (2021).

248. Singh, G. *et al.* An approach to overcome first cycle irreversible capacity in P2-Na2/3[Fe1/2Mn1/2]O2. *Electrochemistry Communications* **37**, 61–63 (2013).

249. Sathiya, M. *et al.* Dual Stabilization and Sacrificial Effect of Na2CO3 for Increasing Capacities of Na-Ion Cells Based on P2-NaxMO2 Electrodes. *Chem. Mater.* **29**, 5948–5956 (2017).

250. Jo, C.-H., Choi, J. U., Yashiro, H. & Myung, S.-T. Controllable charge capacity using a black additive for high-energy-density sodium-ion batteries. *J. Mater. Chem. A* **7**, 3903–3909 (2019).

251. Shanmukaraj, D. *et al.* Highly Efficient, Cost Effective, and Safe Sodiation Agent for High-Performance Sodium-Ion Batteries. *ChemSusChem* **11**, 3286–3291 (2018).

252. Niu, Y.-B. *et al.* High-Efficiency Cathode Sodium Compensation for Sodium-Ion Batteries. *Advanced Materials* **32**, 2001419 (2020).

253. Hu, L. *et al.* Sodium Acetate as Residual-Free Presodiation Additive for Enhancing the Energy Density of Sodium-Ion Batteries. *ACS Energy Lett.* **9**, 1148–1157 (2024).

254. Shen, B. *et al.* Manipulating irreversible phase transition of NaCrO2 towards an effective sodium compensation additive for superior sodium-ion full cells. *Journal of Colloid and Interface Science* **553**, 524–529 (2019).

255. Zhang, B. *et al.* Insertion compounds and composites made by ball milling for advanced sodium-ion batteries. *Nat Commun* **7**, 10308 (2016).

256. Wang, Y. *et al.* On the Practicability of the Solid-State Electrochemical Pre-Sodiation Technique on Hard Carbon Anodes for Sodium-Ion Batteries. *Advanced Functional Materials* **34**, 2403841 (2024).

257. Fang, H. *et al.* Dual-Function Presodiation with Sodium Diphenyl Ketone towards Ultra-stable Hard Carbon Anodes for Sodium-Ion Batteries. *Angewandte Chemie International Edition* **62**, e202214717 (2023).

258. Oh, J. A. S. *et al.* High-Performing All-Solid-State Sodium-Ion Batteries Enabled by the Presodiation of Hard Carbon. *Advanced Energy Materials* **13**, 2300776 (2023).

259. Mirza, S. *et al.* A simple pre-sodiation strategy to improve the performance and energy density of sodium ion batteries with Na4V2(PO4)3 as the cathode material. *J. Mater. Chem. A* **8**, 23368–23375 (2020).

260. Wang, Z. *et al.* Full-Cell Presodiation Strategy to Enable High-Performance Na-Ion Batteries. *Advanced Energy Materials* **13**, 2302514 (2023).

261. Gao, X. *et al.* A Bifuctional Presodiation Reagent for Hard Carbon Anodes Enhancing Performance of Sodium-Ion Batteries. *ACS Energy Lett.* **9**, 1141–1147 (2024).

262. Baggetto, L. *et al.* The local atomic structure and chemical bonding in sodium tin phases. *Journal of Materials Chemistry A* **2**, 18959–18973 (2014).

263. Liu, Z. *et al.* Highly Reversible Sodiation/Desodiation from a Carbon-

Sandwiched SnS2 Nanosheet Anode for Sodium Ion Batteries. *Nano Lett.* **20**, 3844–3851 (2020).

264. Tofoni, A., Tavani, F., Persson, I. & D'Angelo, P. P K-Edge XANES Calculations of Mineral Standards: Exploring the Potential of Theoretical Methods in the Analysis of Phosphorus Speciation. *Inorg. Chem.* **62**, 11188–11198 (2023).

265. Persson, I., Klysubun, W. & Lundberg, D. A K-edge P XANES study of phosphorus compounds in solution. *Journal of Molecular Structure* **1179**, 608–611 (2019).

266. Petric, M. *et al.* Chemical State Analysis of Phosphorus Performed by X-ray Emission Spectroscopy. *Anal. Chem.* **87**, 5632–5639 (2015).

267. Stevens, D. A. & Dahn, J. R. The Mechanisms of Lithium and Sodium Insertion in Carbon Materials. *J. Electrochem. Soc.* **148**, A803 (2001).

268. Stevens, D. A. & Dahn, J. R. An In Situ Small-Angle X-Ray Scattering Study of Sodium Insertion into a Nanoporous Carbon Anode Material within an Operating Electrochemical Cell. *J. Electrochem. Soc.* **147**, 4428 (2000).

269. Kalder, L. *et al.* Empirical correlation of quantified hard carbon structural parameters with electrochemical properties for sodium-ion batteries using a combined WAXS and SANS analysis. *Energy Storage Materials* **67**, 103272 (2024).

270. Sottmann, J. *et al.* Chemical Structures of Specific Sodium Ion Battery Components Determined by Operando Pair Distribution Function and X-ray Diffraction Computed Tomography. *Angewandte Chemie International Edition* **56**, 11385–11389 (2017).

271. Povia, M. *et al.* Operando SAXS/WAXS on the a-P/C as the Anode for Na-Ion Batteries. *J. Phys. Chem. C* **122**, 5917–5923 (2018).

272. Su, Z. *et al.* X-ray Nanocomputed Tomography in Zernike Phase Contrast for Studying 3D Morphology of Li–O_2 Battery Electrode. *ACS Appl. Energy Mater.* **3**, 4093–4102 (2020).

273. Vanpeene, V. *et al.* Dynamics of the Morphological Degradation of Si-Based Anodes for Li-Ion Batteries Characterized by In Situ Synchrotron X-Ray Tomography. *Advanced Energy Materials* **9**, 1803947 (2019).

274. Vanpeene, V., Etiemble, A., Bonnin, A., Maire, E. & Roué, L. In-situ X-ray tomographic study of the morphological changes of a Si/C paper anode for Li-ion batteries. *Journal of Power Sources* **350**, 18–27 (2017).

275. Mu, L. *et al.* Resolving Charge Distribution for Compositionally Heterogeneous Battery Cathode Materials. *Nano Lett.* **22**, 1278–1286 (2022).

276. Lin, F., Zhao, K. & Liu, Y. Heterogeneous Reaction Activities and Statistical Characteristics of Particle Cracking in Battery Electrodes. *ACS Energy Lett.* **6**, 4065–4070 (2021).

277. Lin, T. C. *et al.* Understanding Stabilization in Nanoporous Intermetallic Alloy Anodes for Li-Ion Batteries Using *Operando* Transmission X-ray Microscopy. *ACS Nano* **14**, 14820–14830 (2020).

278. Chao, S.-C. *et al.* In situ transmission X-ray microscopy study on working SnO anode particle of Li-ion batteries. *Journal of The Electrochemical Society* **158**, A1335

(2011).

279. Wang, J., Karen Chen-Wiegart, Y.-C., Eng, C., Shen, Q. & Wang, J. Visualization of anisotropic-isotropic phase transformation dynamics in battery electrode particles. *Nature communications* **7**, 12372 (2016).

280. Lim, J. *et al.* Origin and hysteresis of lithium compositional spatiodynamics within battery primary particles. *Science* **353**, 566–571 (2016).

281. Sun, Y. *et al.* Operando real-space imaging of a structural phase transformation in the high-voltage electrode LixNi0.5Mn1.5O4. *Nat Commun* **15**, 10783 (2024).

282. Xue, Z. *et al.* Asynchronous domain dynamics and equilibration in layered oxide battery cathode. *Nat Commun* **14**, 8394 (2023).

283. Richards, D., Zayats, A., Keilmann, F. & Hillenbrand, R. Near-field microscopy by elastic light scattering from a tip. *Philosophical Transactions of the Royal Society of London. Series A: Mathematical, Physical and Engineering Sciences* **362**, 787–805 (2004).

284. Hillenbrand, R., Taubner, T. & Keilmann, F. Phonon-enhanced light–matter interaction at the nanometre scale. *Nature* **418**, 159–162 (2002).

285. Huth, F. *et al.* Nano-FTIR Absorption Spectroscopy of Molecular Fingerprints at 20 nm Spatial Resolution. *Nano Lett.* **12**, 3973–3978 (2012).

286. Hillenbrand, R., Abate, Y., Liu, M., Chen, X. & Basov, D. N. Visible-to-THz near-field nanoscopy. *Nat Rev Mater* **10**, 285–310 (2025).

287. Larson, J. M., Dopilka, A. & Kostecki, R. Infrared nanoimaging and nanospectroscopy of electrochemical energy storage materials and interfaces. *Current Opinion in Electrochemistry* **47**, 101548 (2024).

288. He, X., Larson, J. M., Bechtel, H. A. & Kostecki, R. In situ infrared nanospectroscopy of the local processes at the Li/polymer electrolyte interface. *Nat Commun* **13**, 1398 (2022).

289. Dopilka, A., Gu, Y., Larson, J. M., Zorba, V. & Kostecki, R. Nano-FTIR Spectroscopy of the Solid Electrolyte Interphase Layer on a Thin-Film Silicon Li-Ion Anode. *ACS Appl. Mater. Interfaces* **15**, 6755–6767 (2023).

290. Dopilka, A., Larson, J. M. & Kostecki, R. Operando Infrared Nanospectroscopy of the Silicon/Electrolyte Interface during Initial Stages of Solid-Electrolyte-Interphase Layer Formation. *ACS Energy Lett.* **10**, 410–419 (2025).

291. Dopilka, A., Larson, J. M., Cha, H. & Kostecki, R. Synchrotron Near-Field Infrared Nanospectroscopy and Nanoimaging of Lithium Fluoride in Solid Electrolyte Interphases in Li-Ion Battery Anodes. *ACS Nano* **18**, 15270–15283 (2024).

292. Wehmeier, L. *et al.* Ultrabroadband Terahertz Near-Field Nanospectroscopy with a HgCdTe Detector. *ACS Photonics* **10**, 4329–4339 (2023).

293. Chang, I. F. & Mitra, S. S. Temperature Dependence of Long-Wavelength Optic Phonons of NaF Single Crystals. *Phys. Rev. B* **5**, 4094–4101 (1972).

294. McArthur, M. A., Trussler, S. & Dahn, J. R. In Situ Investigations of SEI Layer Growth on Electrode Materials for Lithium-Ion Batteries Using Spectroscopic

Ellipsometry. *J. Electrochem. Soc.* **159**, A198 (2011).

295. Lucas, I. T., Syzdek, J. & Kostecki, R. Interfacial processes at single-crystal β-Sn electrodes in organic carbonate electrolytes. *Electrochemistry Communications* **13**, 1271–1275 (2011).

296. Kong, F. *et al.* In situ studies of SEI formation. *Journal of Power Sources* **97–98**, 58–66 (2001).

297. Beattie, S. D., Hatchard, T., Bonakdarpour, A., Hewitt, K. C. & Dahn, J. R. Anomalous, High-Voltage Irreversible Capacity in Tin Electrodes for Lithium Batteries. *J. Electrochem. Soc.* **150**, A701 (2003).

298. Zhang, B., Ghimbeu, C. M., Laberty, C., Vix-Guterl, C. & Tarascon, J.-M. Correlation Between Microstructure and Na Storage Behavior in Hard Carbon. *Advanced Energy Materials* **6**, 1501588 (2016).

299. Bai, P. *et al.* Elucidation of the Sodium-Storage Mechanism in Hard Carbons. *Advanced Energy Materials* **8**, 1703217 (2018).

300. Zhang, Z. *et al.* Resolving three-dimensional nanoscale heterogeneities in lithium metal batteries with cryoelectron tomography. *Matter* **8**, (2025).

301. Sun, B. *et al.* Closed Pore Architecture and Sodium Cluster Deposit Visualization in Hard Carbon. *Nano Lett.* **25**, 7161–7169 (2025).

302. Li, Y. *et al.* Atomic structure of sensitive battery materials and interfaces revealed by cryo–electron microscopy. *Science* **358**, 506–510 (2017).

303. Xie, H. *et al.* β-SnSb for Sodium Ion Battery Anodes: Phase Transformations

Responsible for Enhanced Cycling Stability Revealed by In Situ TEM. *ACS Energy Lett.* **3**, 1670–1676 (2018).

304. Lu, X. *et al.* Germanium as a Sodium Ion Battery Material: In Situ TEM Reveals Fast Sodiation Kinetics with High Capacity. *Chem. Mater.* **28**, 1236–1242 (2016).

305. Gao, L. *et al.* Revealing the chemistry of an anode-passivating electrolyte salt for high rate and stable sodium metal batteries. *J. Mater. Chem. A* **6**, 12012–12017 (2018).

306. Gao, L., Chen, J., Chen, Q. & Kong, X. The chemical evolution of solid electrolyte interface in sodium metal batteries. *Science Advances* **8**, eabm4606 (2022).

307. Bray, J. M. *et al.* Operando visualisation of battery chemistry in a sodium-ion battery by 23Na magnetic resonance imaging. *Nat Commun* **11**, 2083 (2020).

308. Liu, X. *et al.* Solid-State NMR and MRI Spectroscopy for Li/Na Batteries: Materials, Interface, and In Situ Characterization. *Advanced Materials* **33**, 2005878 (2021).

309. Geisler, J., Pfeiffer, L., A. Ferrero, G., Axmann, P. & Adelhelm, P. Setup Design and Data Evaluation for DEMS in Sodium Ion Batteries, Demonstrated on a Mn-Rich Cathode Material. *Batteries & Supercaps* **7**, e202400006 (2024).

310. Zhang, H. *et al.* Full-Dimensional Analysis of Gaseous Products Within Li-Ion Batteries by On-Line GC-BID/MS. *Advanced Energy Materials* **14**, 2400397 (2024).

311. Deng, X. *et al.* Abnormal Gas Generation during First Discharge Process of Sodium Ion Battery. *Angewandte Chemie International Edition* **63**, e202412222 (2024).

312. Xue, J. *et al.* Unlocking the Na-Storage Behavior in Hard Carbon Anode by Mass Spectrometry. *Nano Lett.* **24**, 9839–9845 (2024).

313. Liu, W. *et al.* Gassing in Sn-Anode Sodium-Ion Batteries and Its Remedy by Metallurgically Prealloying Na. *ACS Appl. Mater. Interfaces* **11**, 23207–23212 (2019).

314. Gong, C. *et al.* The role of an elastic interphase in suppressing gas evolution and promoting uniform electroplating in sodium metal anodes. *Energy & Environmental Science* **16**, 535–545 (2023).

315. Liu, S. *et al.* Hollow nanoporous red phosphorus as an advanced anode for sodium-ion batteries. *Journal of Materials Chemistry A* **6**, 12992–12998 (2018).

316. Tian, W., Wang, L., Huo, K. & He, X. Red phosphorus filled biomass carbon as high-capacity and long-life anode for sodium-ion batteries. *Journal of Power Sources* **430**, 60–66 (2019).

317. Qian, J. *et al.* High capacity Na-storage and superior cyclability of nanocomposite Sb/C anode for Na-ion batteries. *Chemical Communications* **48**, 7070–7072 (2012).

318. Darwiche, A. *et al.* Better Cycling Performances of Bulk Sb in Na-Ion Batteries Compared to Li-Ion Systems: An Unexpected Electrochemical Mechanism. *J. Am. Chem. Soc.* **134**, 20805–20811 (2012).

319. Su, D., Dou, S. & Wang, G. Bismuth: A new anode for the Na-ion battery. *Nano Energy* **12**, 88–95 (2015).

a

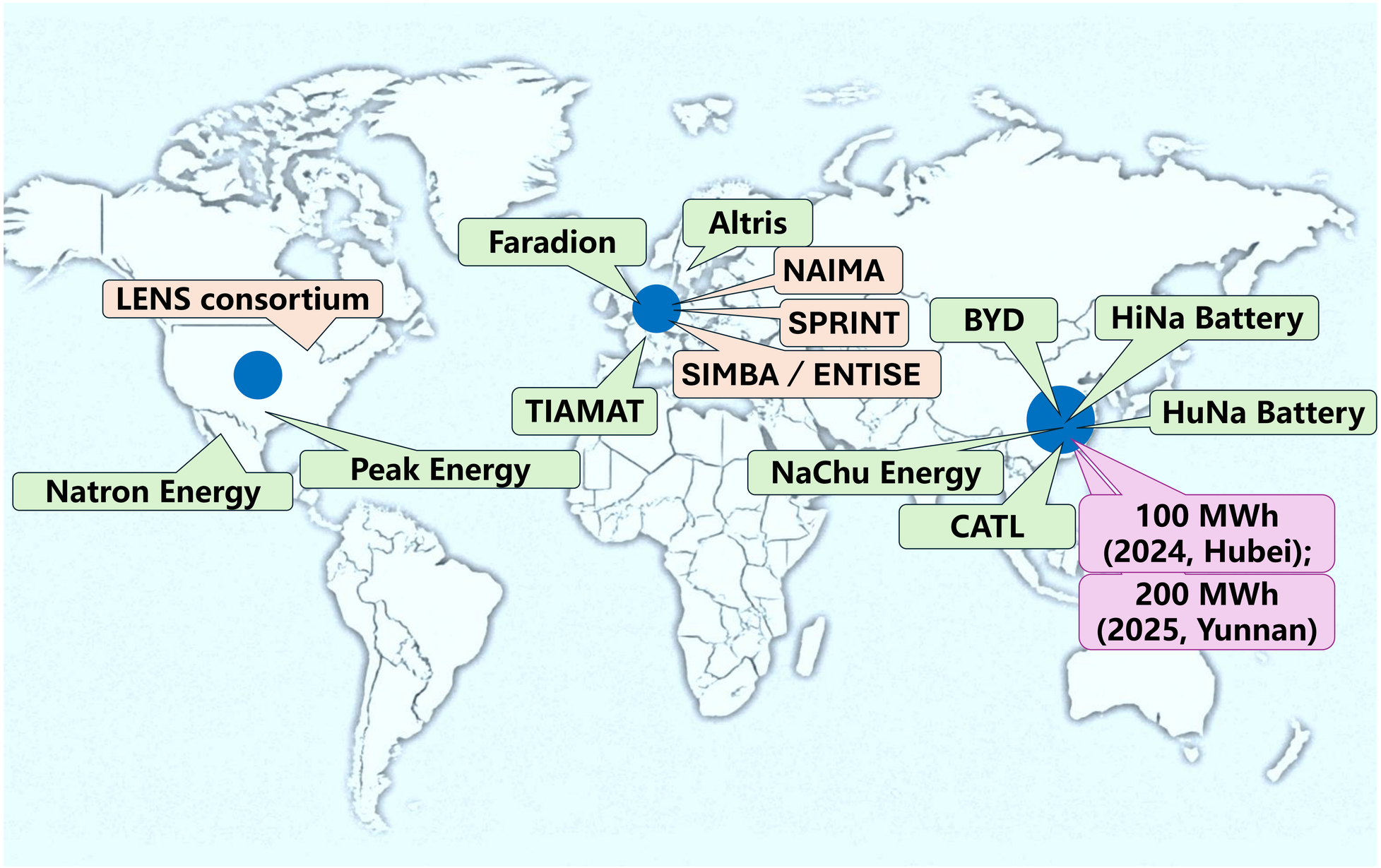
Faradion
Altris
NAIMA
SPRINT
SIMBA / ENTISE
LENS consortium
TIAMAT
Peak Energy
Natron Energy
BYD
HiNa Battery
HuNa Battery
NaChu Energy
CATL
100 MWh (2024, Hubei);
200 MWh (2025, Yunnan)
Major Project
Industrial Company
Deployment

b

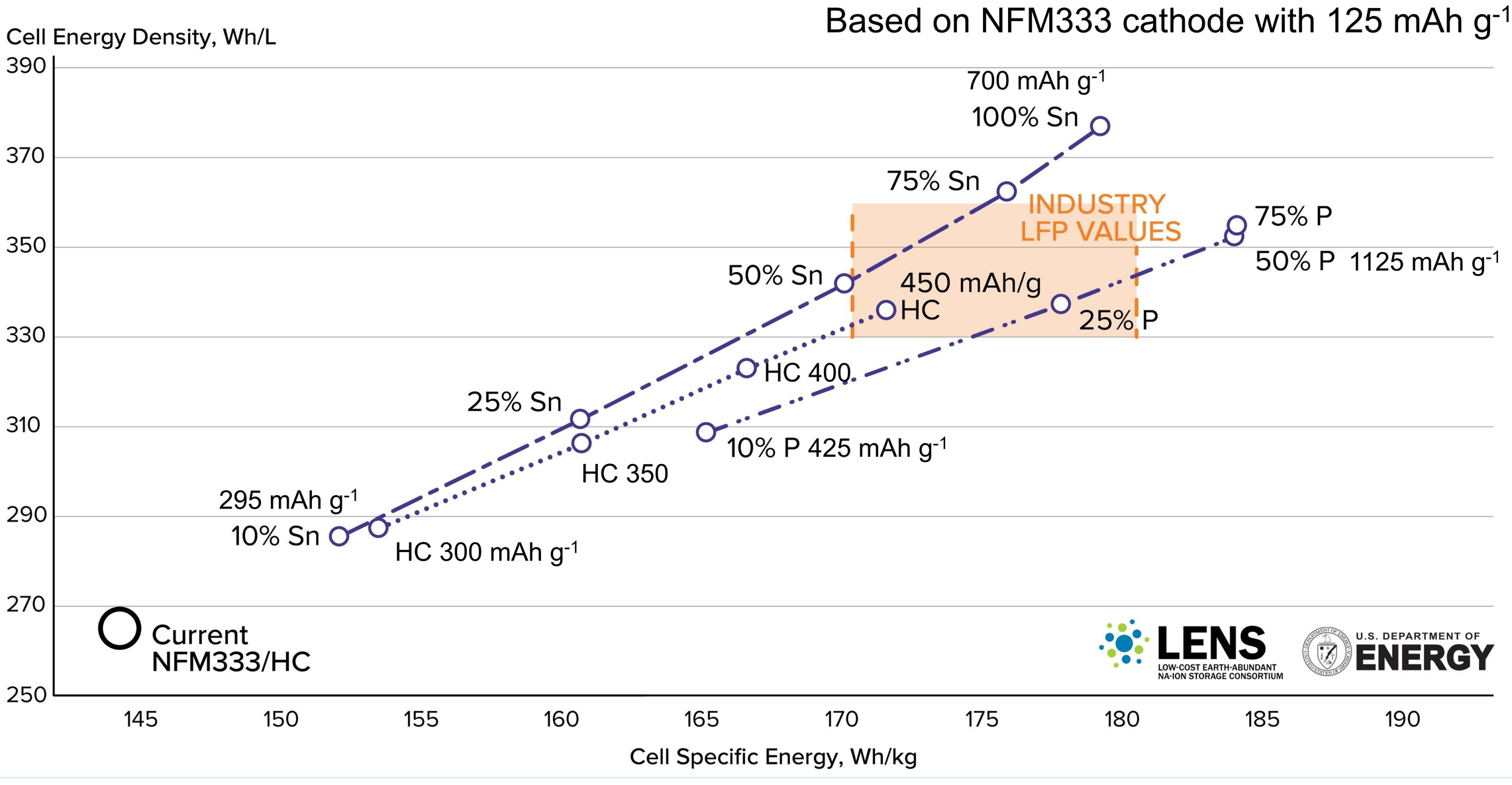
Based on NFM333 cathode with 125 mAh g-1
Cell Energy Density, Wh/L
390
370
350
330
310
290
270
250
700 mAh g-1
100% Sn
75% Sn
INDUSTRY LFP VALUES
75% P
50% P 1125 mAh g-1
50% Sn
450 mAh/g HC
25% P
HC 400
25% Sn
HC 350
10% P 425 mAh g-1
295 mAh g-1
10% Sn
HC 300 mAh g-1
Current NFM333/HC
LENS
LOW-COST EARTH-ABUNDANT NA-ION STORAGE CONSORTIUM
U.S. DEPARTMENT OF ENERGY
145
150
155
160
165
170
175
180
185
190
Cell Specific Energy, Wh/kg

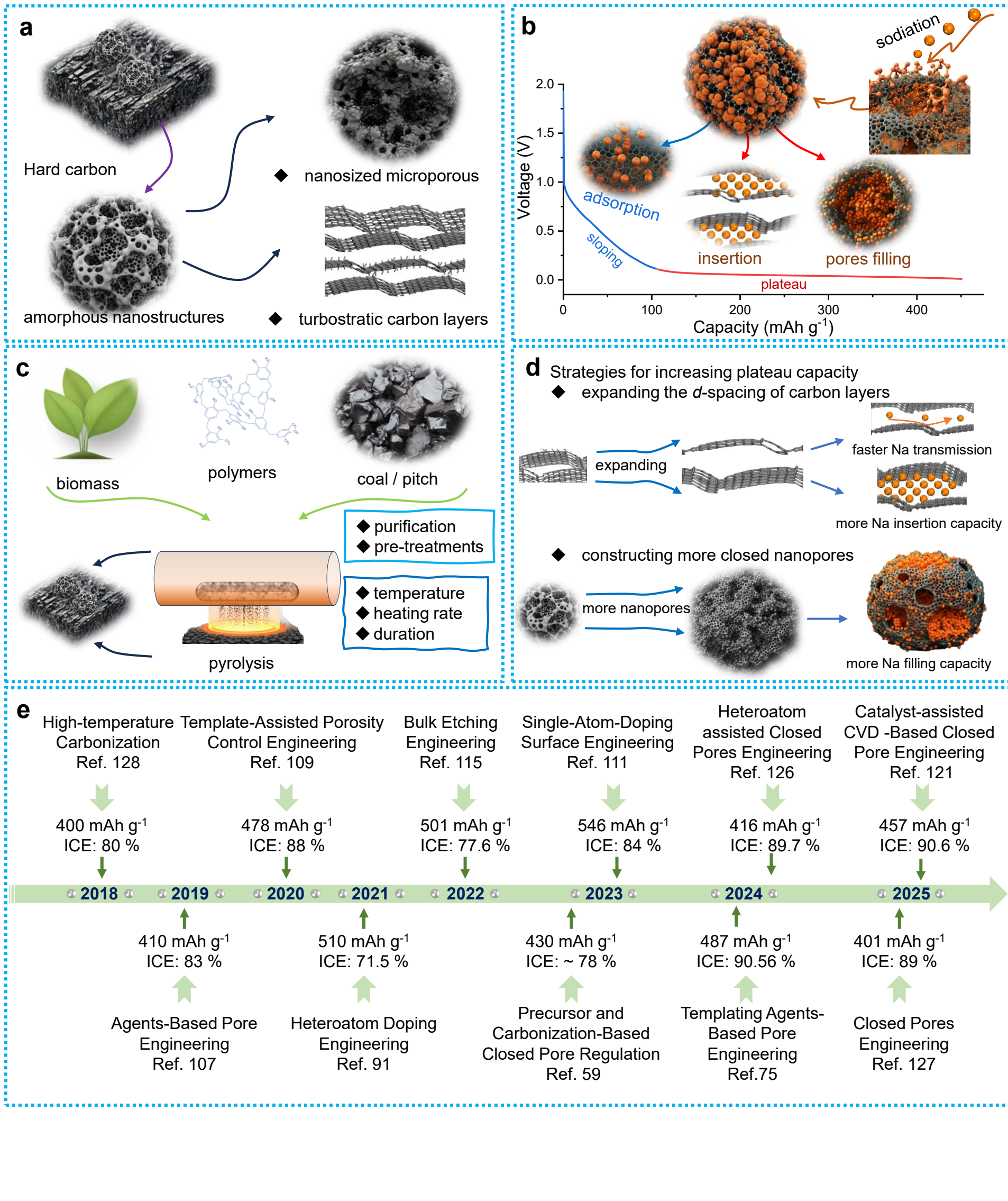
a
Hard carbon
nanosized microporous
amorphous nanostructures
turbostratic carbon layers
b
sodiation
adsorption
sloping
insertion
pores filling
plateau
Voltage (V)
Capacity (mAh g-1)
c
biomass
polymers
coal / pitch
purification
pre-treatments
temperature
heating rate
duration
pyrolysis
d
Strategies for increasing plateau capacity
expanding the d-spacing of carbon layers
expanding
faster Na transmission
more Na insertion capacity
constructing more closed nanopores
more nanopores
more Na filling capacity
e
High-temperature Carbonization Ref. 128
400 mAh g-1 ICE: 80 %
2018
Agents-Based Pore Engineering Ref. 107
410 mAh g-1 ICE: 83 %
2019
Template-Assisted Porosity Control Engineering Ref. 109
478 mAh g-1 ICE: 88 %
2020
Heteroatom Doping Engineering Ref. 91
510 mAh g-1 ICE: 71.5 %
2021
Bulk Etching Engineering Ref. 115
501 mAh g-1 ICE: 77.6 %
2022
Single-Atom-Doping Surface Engineering Ref. 111
546 mAh g-1 ICE: 84 %
2023
Precursor and Carbonization-Based Closed Pore Regulation Ref. 59
430 mAh g-1 ICE: ~ 78 %
Heteroatom assisted Closed Pores Engineering Ref. 126
416 mAh g-1 ICE: 89.7 %
2024
Templating Agents-Based Pore Engineering Ref.75
487 mAh g-1 ICE: 90.56 %
Catalyst-assisted CVD -Based Closed Pore Engineering Ref. 121
457 mAh g-1 ICE: 90.6 %
2025
Closed Pores Engineering Ref. 127
401 mAh g-1 ICE: 89 %

a Hard carbon

b Red P

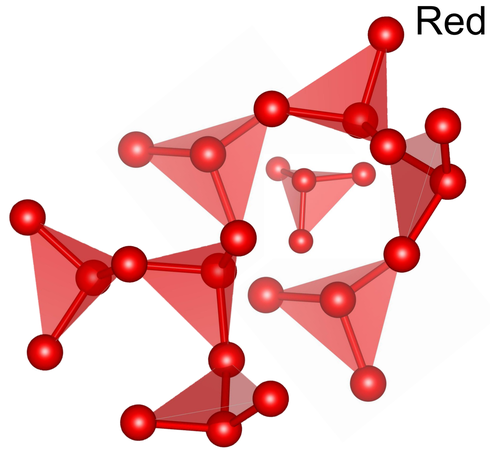

c Black P

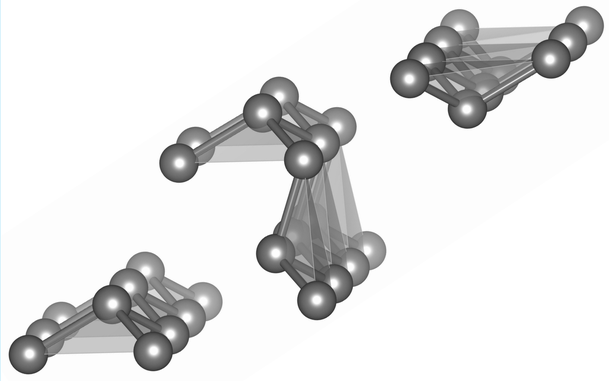

Space group: Cmca

d Ge

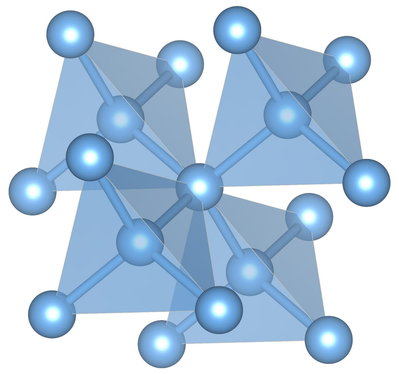

Space group: Fd3̄m

e Sn

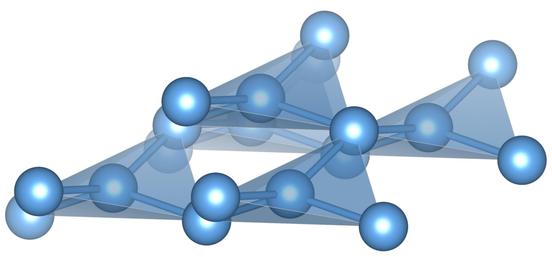

Space group: I4̄1/amd

f Sb

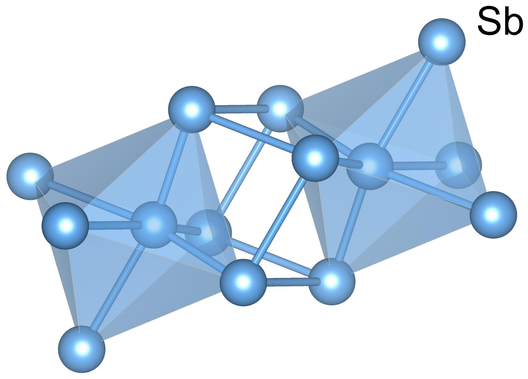

Space group: R3̄m

g Pb

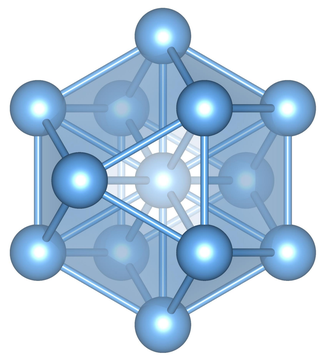

Space group: Fm3̄m

h Bi

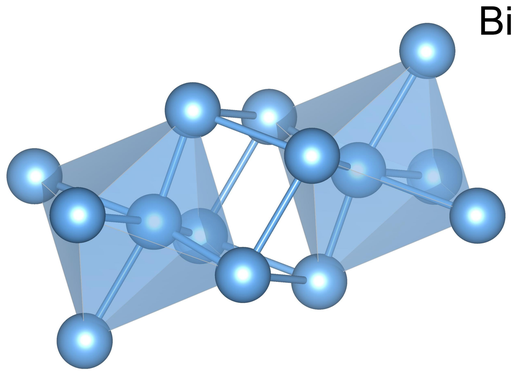

Space group: R3̄m

i Natural abundancy (ppm)

j Production per year (t/year)

Figure 4

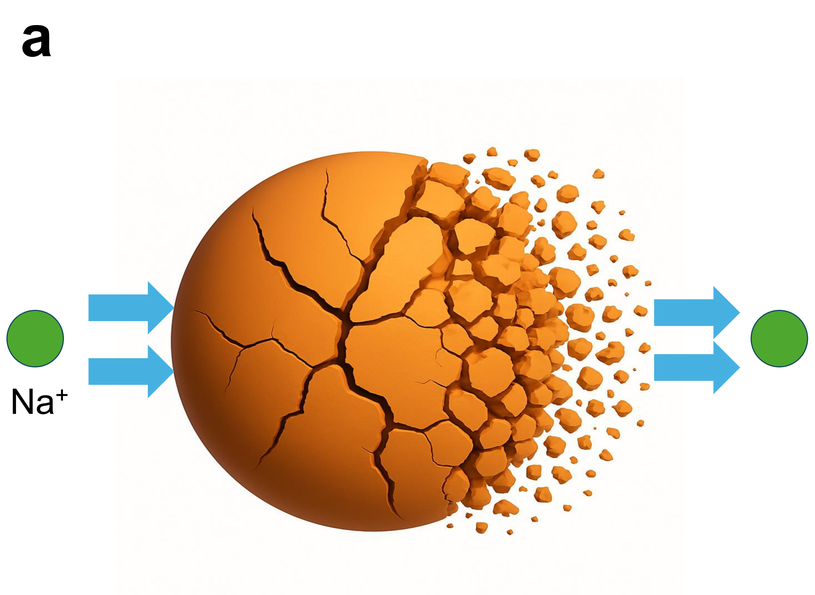

Bulk alloy: Severe volume change leads to cracks, fractures and pulverization

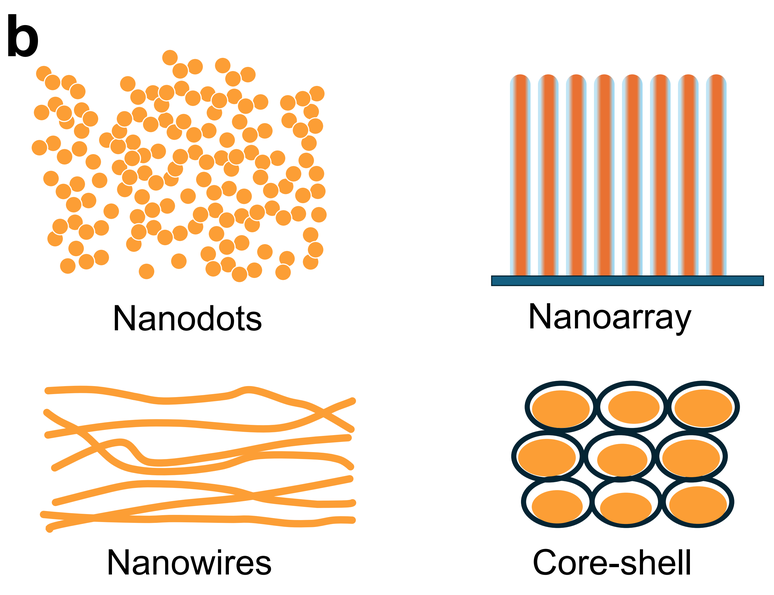

Nano-engineering: Short diffusion paths, enhanced mechanical resilience

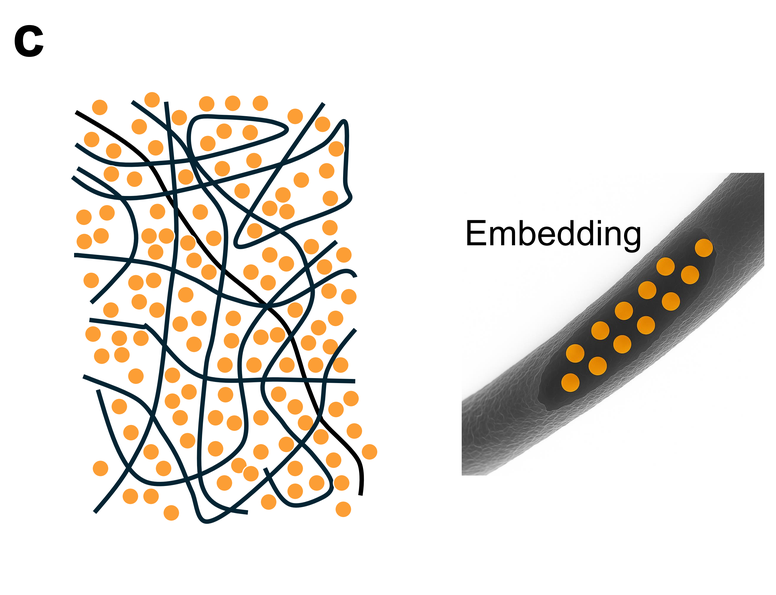

Alloy@C composite: Ensuring conductivity, protecting surface, maintaining structural stability

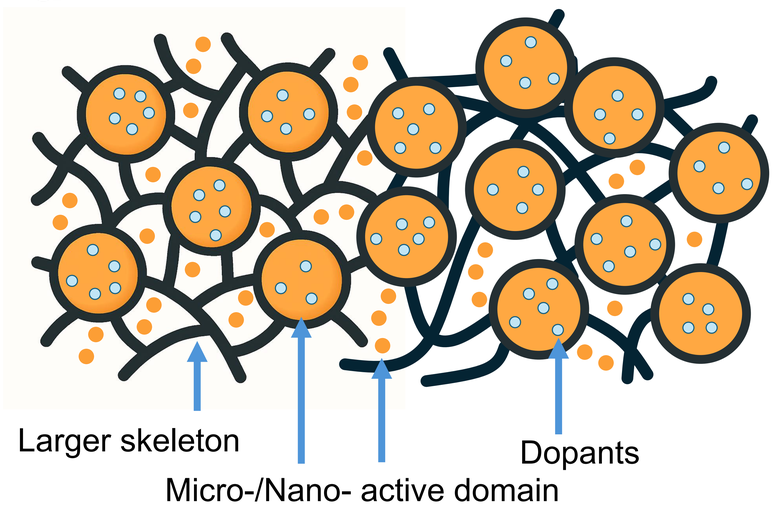

Micro-engineering: Multi-scale design for reversible volume change and durability

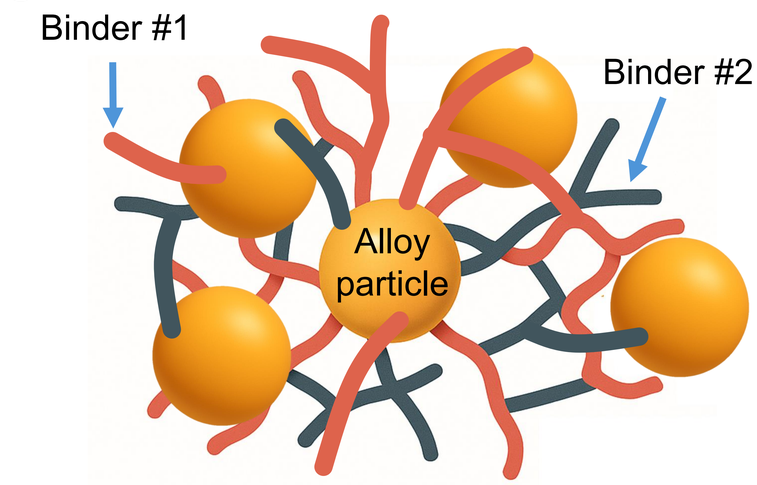

Hybrid binders: Enhancing mechanical stability via polymer networks

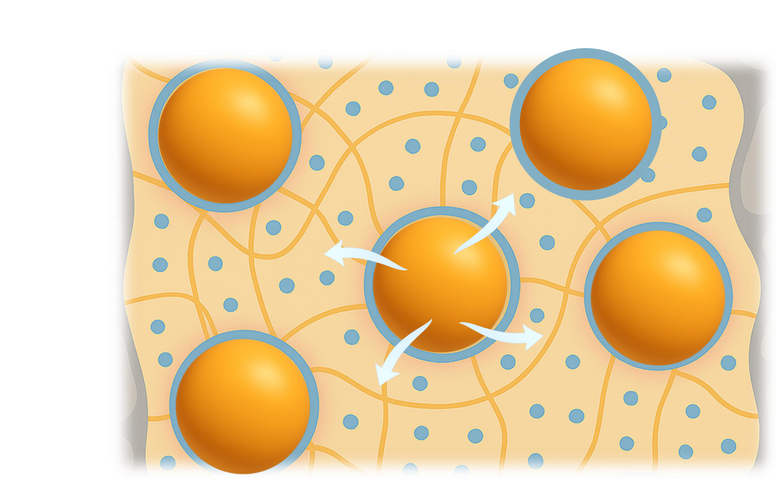

GPE strategy: Facilitating ion transport and suppressing interfacial degradation

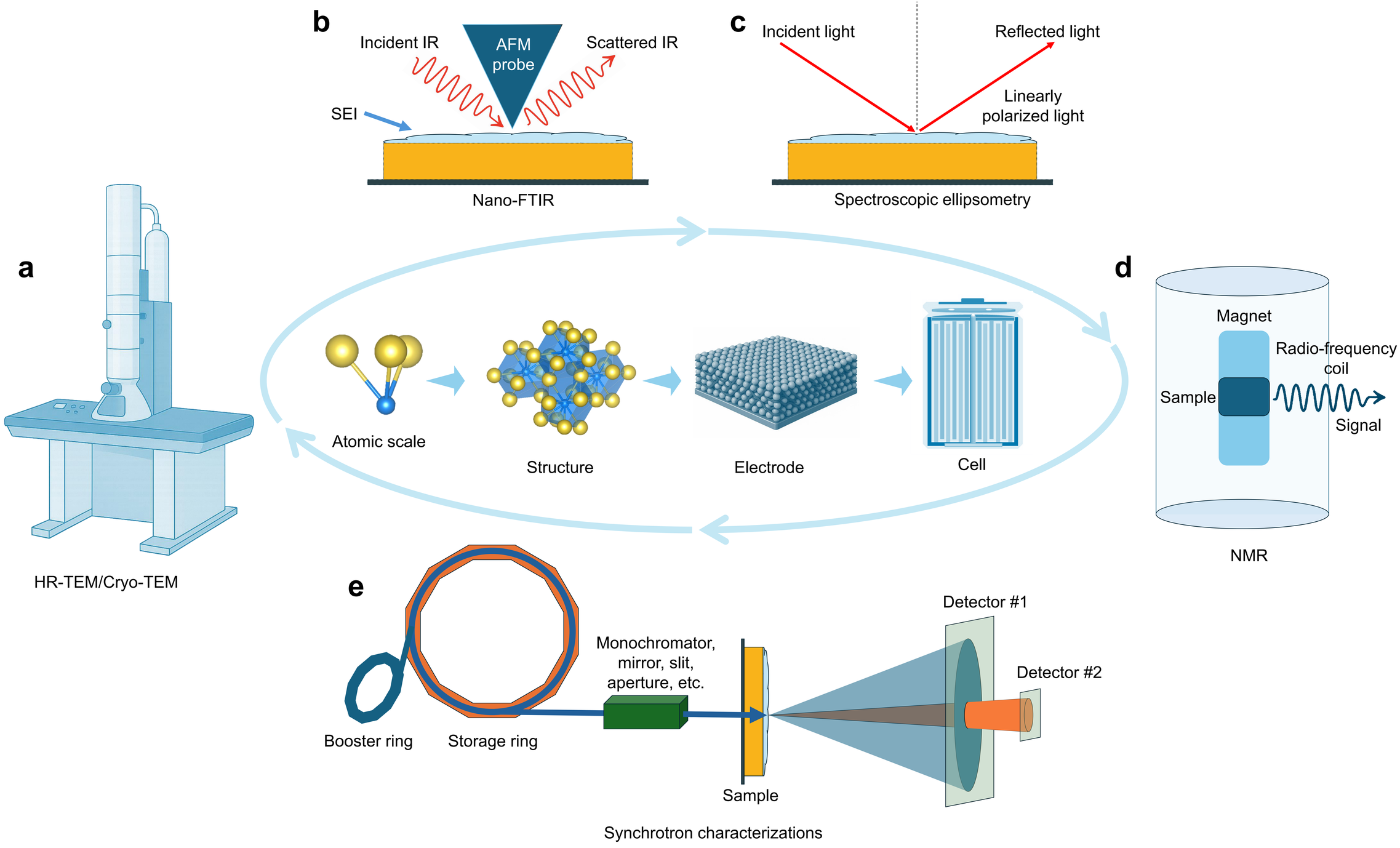
b
Incident IR
AFM probe
Scattered IR
SEI
Nano-FTIR
c
Incident light
Reflected light
Linearly polarized light
Spectroscopic ellipsometry
a
Atomic scale
Structure
Electrode
Cell
HR-TEM/Cryo-TEM
d
Magnet
Radio-frequency coil
Sample
Signal
NMR
e
Booster ring
Storage ring
Monochromator, mirror, slit, aperture, etc.
Sample
Detector #1
Detector #2
Synchrotron characterizations